Virology 432 (2012) 29–38

Contents lists available at SciVerse ScienceDirect

Virology

journal homepage: www.elsevier.com/locate/yviro

Trans-complemented hepatitis C virus particles as a versatile tool for study of virus assembly and infection

Ryosuke Suzuki [a,*], Kenji Saito [a], Takanobu Kato [a], Masayuki Shirakura [b], Daisuke Akazawa [a], Koji Ishii [a], Hideki Aizaki [a], Yumi Kanegae [c], Yoshiharu Matsuura [d], Izumu Saito [c], Takaji Wakita [a], Tetsuro Suzuki [e,**]

[a] *Department of Virology II, National Institute of Infectious Diseases, 1-23-1 Toyama, Shinjuku-ku, Tokyo 162-8640, Japan*
[b] *Influenza Virus Research Center, National Institute of Infectious Diseases, Tokyo 208-0011, Japan*
[c] *Institute of Medical Science, University of Tokyo, Tokyo 108-8639, Japan*
[d] *Research Institute for Microbial Diseases, Osaka University, Osaka 565-0871, Japan*
[e] *Department of Infectious Diseases, Hamamatsu University School of Medicine, 1-20-1 Handayama, Higashi-ku, Hamamatsu, Shizuoka 431-3192, Japan*

ARTICLE INFO

Article history:
Received 30 March 2012
Returned to author for revisions
23 April 2012
Accepted 25 May 2012
Available online 22 June 2012

Keywords:
HCV
HCVtcp
Trans-packaging
Single-round infection

ABSTRACT

In this study, we compared the entry processes of *trans*-complemented hepatitis C virus particles (HCVtcp), cell culture-produced HCV (HCVcc) and HCV pseudoparticles (HCVpp). Anti-CD81 antibody reduced the entry of HCVtcp and HCVcc to almost background levels, and that of HCVpp by approximately 50%. Apolipoprotein E-dependent infection was observed with HCVtcp and HCVcc, but not with HCVpp, suggesting that the HCVtcp system is more relevant as a model of HCV infection than HCVpp. We improved the productivity of HCVtcp by introducing adapted mutations and by deleting sequences not required for replication from the subgenomic replicon construct. Furthermore, blind passage of the HCVtcp in packaging cells resulted in a novel mutation in the NS3 region, N1586D, which contributed to assembly of infectious virus. These results demonstrate that our plasmid-based system for efficient production of HCVtcp is beneficial for studying HCV life cycles, particularly in viral assembly and infection.

Introduction

Over 170 million people worldwide are chronically infected with hepatitis C virus (HCV), and are at risk of developing chronic liver diseases (Hoofnagle, 2002). HCV is an enveloped virus of the family *Flaviviridae*, and its genome is a positive-strand RNA consisting of the 5′-untranslated region (UTR), an open reading frame encoding viral proteins (core, E1, E2, p7, NS2, NS3, NS4A, NS4B, NS5A, and NS5B) and the 3′-UTR (Suzuki et al., 2007).

Host–virus interactions are required during the initial steps of viral infection. It was previously reported that CD81 (Bartosch et al., 2003a, b; McKeating et al., 2004; Pileri et al., 1998), scavenger receptor class B type I (Bartosch et al., 2003a, b; Scarselli et al., 2002), claudin-1 (Evans et al., 2007; Liu et al., 2009) and occludin (Benedicto et al., 2009; Evans et al., 2007; Liu et al., 2009; Ploss et al., 2009) are critical molecules for HCV entry into cells. CD81 interacts with HCV E2 via a second extracellular loop (Bartosch et al., 2003a, b; Hsu et al., 2003) and its role in the internalization process was confirmed (Cormier et al., 2004; Flint et al., 2006). It has also been shown that infectious HCV particles produced in cell cultures (HCVcc) exist as apolipoprotein E (ApoE)-enriched lipoprotein particles (Chang et al., 2007) and that ApoE is important for HCV infectivity (Owen et al., 2009).

Investigation of HCV had been hampered by difficulties in amplifying the virus in vitro before development of robust cell culture systems based on JFH-1 isolates (Lindenbach et al., 2005; Wakita et al., 2005; Zhong et al., 2005). Retrovirus-based HCV pseudoparticles (HCVpp), in which cell entry is dependent on HCV glycoproteins, have been used to study virus entry (Bartosch et al., 2003a; Hsu et al., 2003). Vesicular stomatitis virus (VSV)-based pseudotypic viruses bearing HCV E1 and E2 and replication-competent recombinant VSV encoding HCV envelopes have also been available as surrogate models for studies of HCV infection (Mazumdar et al., 2011; Tani et al., 2007).

It was recently shown that HCV subgenomic replicons can be packaged when structural proteins are supplied in *trans* (Adair et al., 2009; Ishii et al., 2008; Masaki et al., 2010; Steinmann et al., 2008). These *trans*-complemented HCV particles (HCVtcp) are infectious, but support only single-round infection and are unable to spread. Establishment of flexible systems to efficiently produce HCVtcp should contribute to studying HCV assembly, in particular encapsidation of the viral genome, and entry to cells with less stringent biosafety and biosecurity measures. Although single-round infection can be achieved by using the HCVcc system with receptor knock-out

* Corresponding author. Fax: +81 3 5285 1161.
** Corresponding author. Fax: +81 53 435 2338.
E-mail addresses: ryosuke@nih.go.jp (R. Suzuki), tesuzuki@hama-med.ac.jp (T. Suzuki).

0042-6822/$ - see front matter © 2012 Elsevier Inc. All rights reserved.
http://dx.doi.org/10.1016/j.virol.2012.05.033

cells, the single-round HCVcc system is not suitable for studying virus entry. We previously described plasmid-based production of HCVcc and HCVtcp (Masaki et al., 2010). Here, we demonstrated that HCVtcp production can be enhanced by introducing the previously reported cell-culture adaptive mutations and by deleting sequences not essential for replication in the subgenomic replicon construct. By providing genotype 1b-derived core-to-p7 in addition to intragenotypic viral proteins, chimeric HCVtcp were generated. Furthermore, blind passage of HCVtcp in the packaging cells resulted in the identification of a novel cell culture-adaptive mutation in NS3 that enables us to establish the efficient production of HCVtcp with structural proteins from various strains. Taken together, our system for producing single-cycle infectious HCV particles should be useful in the study of entry and assembly steps of the HCV life cycles. This technology may also have potential to be the basis for the safer vaccine development.

Results

Enhancement of HCVtcp production by adaptive mutations in E2, p7 and NS2 and by deleting sequences not essential for replication from replicon construct

In our HCVtcp system, the RNA polymerase I (Pol I)-driven replicon plasmid, which carries a dicistronic subgenomic luciferase reporter replicon of JFH-1 strain with a Pol I promoter and terminator (pHH/SGR-Luc), as well as a plasmid containing core-NS2 cDNA under the CAG promoter (pCAGC-NS2) were used (Masaki et al., 2010). In an effort to improve the yield of HCVtcp production, cell culture-adaptive mutations in E2 (N417S), p7 (N765D) and NS2 (Q1012R) which were previously selected from serial passage of HCVcc (Russell et al., 2008) were introduced into the core-NS2 expression plasmid (Fig. 1A) (residues are numbered

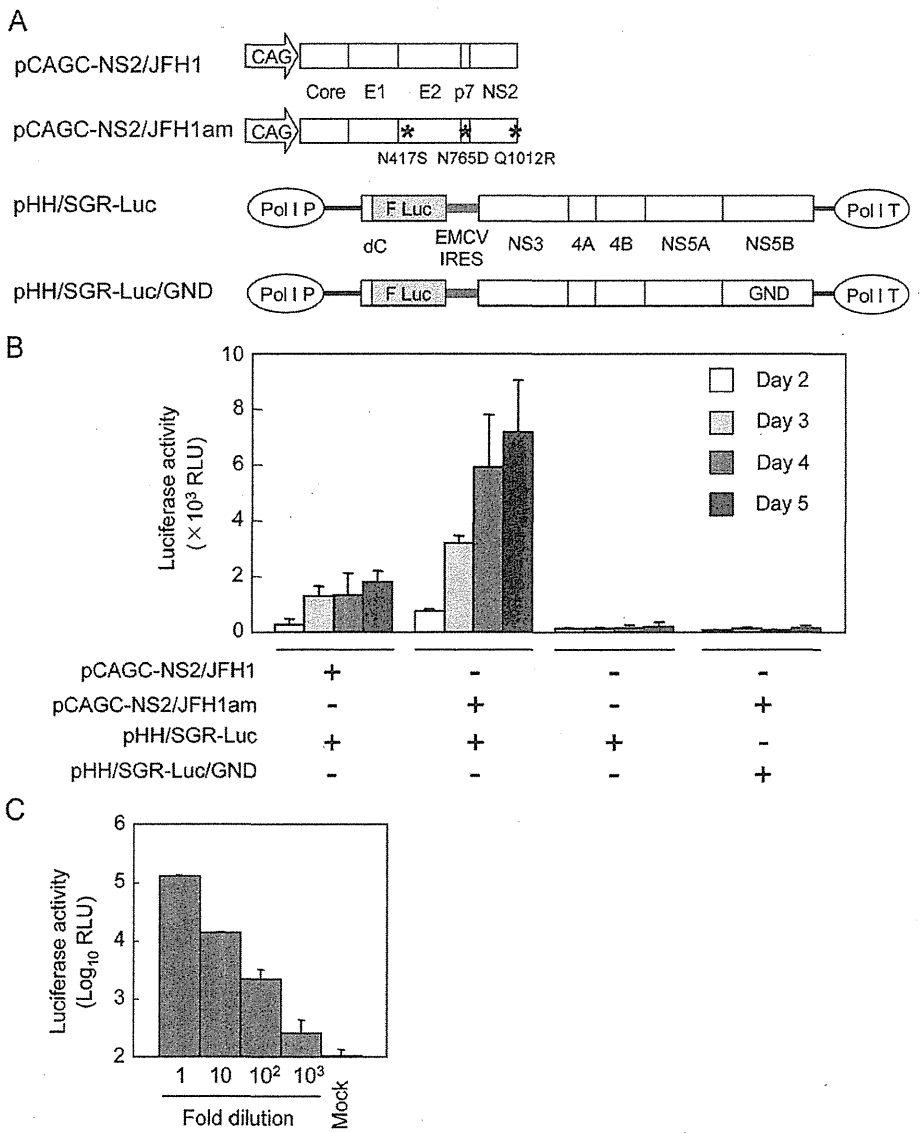

Fig. 1. HCVtcp production by two-plasmid transfection. (A) Schematic representation of plasmids is shown. HCV polyproteins derived from JFH-1 are indicated by white boxes. HCV UTRs are indicated by bold lines. The internal ribosomal entry site from encephalomyocarditis virus (EMCV IRES) is denoted as gray lines. Adaptive mutations are indicated as asterisks. F Luc: firefly luciferase gene; CAG: CAG promoter; Pol I P: RNA polymerase I promoter; Pol I T: RNA polymerase I terminator; GND: replication-deficient GND mutation. (B) Luciferase activity in Huh7.5.1 cells inoculated with supernatant from cells transfected with indicated plasmids at the indicated time points. Data are averages of triplicate values with error bars showing standard deviations. (C) Luciferase activity in cells inoculated with serially diluted HCVtcp.

according to positions within the JFH-1 polyprotein). Supernatants of cells transfected with plasmids (Fig. 1A) were collected and were used to infect Huh7.5.1 cells, which were analyzed by luciferase assay. Introduction of adaptive mutations (pCAGC-NS2/JFH1am) resulted in more than 4-fold higher production of HCVtcp at 5 day post-transfection, as compared to wild-type (WT) (pCAGC-NS2/JFH1) (Fig. 1B), indicating that the adaptive mutations contribute to enhancing HCVtcp production. To confirm that luciferase activity levels in HCVtcp-infected cells are correlated with the number of infectious particles, Huh7.5.1 cells were inoculated with serial dilutions of HCVtcp. Luciferase activity was well correlated with viral load (Fig. 1C), indicating that luciferase assay in HCVtcp-infected cells can be used to quantify HCV infection.

In order to further explore the efficient production of HCVtcp, we generated replicon constructs that lack the luciferase gene or include the partial coding sequences for structural proteins instead of reporter (Fig. 2A). Replication of each replicon in plasmid-transfected cells was then assessed by Western blotting (Fig. 2B). Among the constructs tested, NS5B levels were lowest in cells expressing pHH/SGR-Luc. NS5B levels in cells replicating other replicons appeared to be comparable. Cells were infected with supernatants of cells transfected with each replicon plasmid, along with pCAGC-NS2/JFH1am, followed by infectious unit assay (Fig. 2C). The highest production of HCVtcp was obtained from cells transfected with pHH/SGR, where the luciferase sequence was deleted from pHH/SGR-Luc, thus suggesting that deletion of the sequence not essential for RNA replication in the replicon may contribute to enhancing HCVtcp production.

Production of chimeric HCVtcp by providing heterologous core-p7

In order to elucidate whether *trans*-encapsidation of JFH-1 replicon can be achieved by providing core-p7 from other HCV strains, core-NS2 plasmids were constructed (Fig. 3A). In these plasmids, core through the N-terminal 33 aa of NS2, which contains transmembrane domain 1 of NS2, was derived from either H77c (genotype 1a), THpa (genotype 1b), Con1 (genotype 1b) or J6 (genotype 2a) strain. Residual NS2 was derived from JFH-1, as described previously (Pietschmann et al., 2006). HCVtcp was efficiently produced by core-p7 of J6 and THpa strains, but its production was less efficient in the case of Con1 strain. *Trans*-packaging was not detectable when core-p7 of H77c strain was used (Fig. 3C). Among HCV strains tested, difference in luciferase activity levels in HCVtcp-infected cells (Fig. 3C) were in agreement with that in the viral RNA levels in the culture supernatants of the transfected cells (Fig. 3B). Although the efficacy of *trans*-complementation was variable among strains, chimeric HCVtcp can be generated by providing genotype 1b-derived core-p7 in addition to intragenotypic viral proteins, and was used in subsequent studies.

ApoE- and CD81-dependent infection by HCVtcp

There is accumulating evidence that apolipoproteins, particularly ApoE, contribute to HCV production and infectivity (Chang et al., 2007; Owen et al., 2009). To determine whether ApoE is involved in infection of target cells by HCVtcp, we infected cells in the presence of increasing concentrations of anti-ApoE antibody.

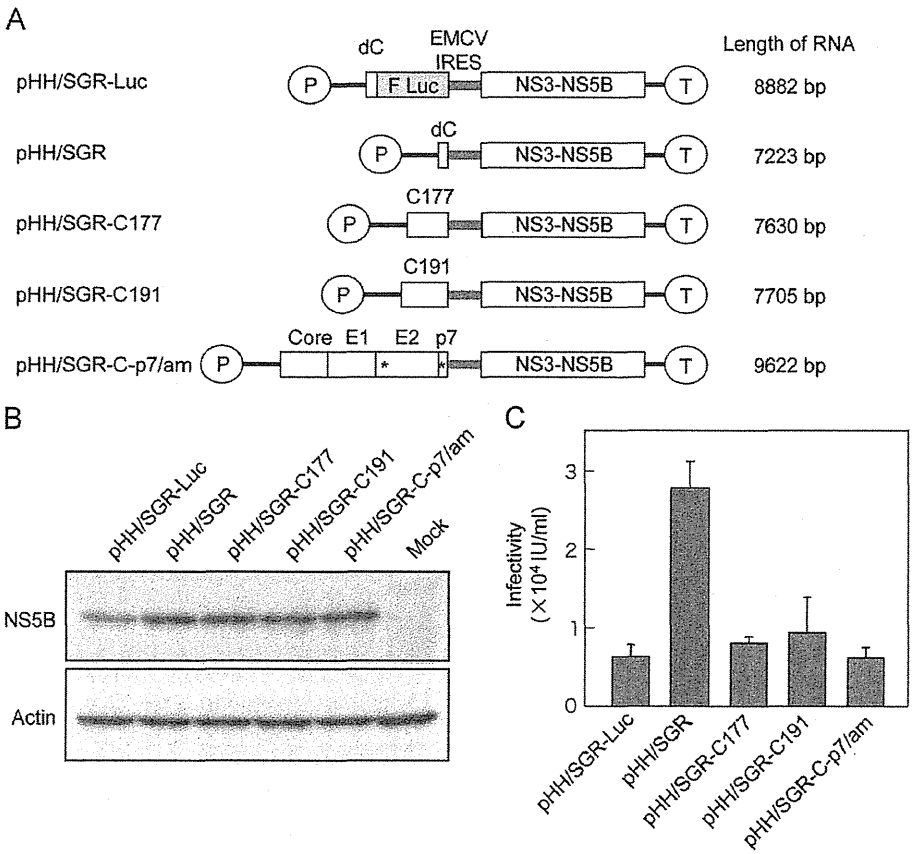

Fig. 2. Production of HCVtcp with different replicon constructs. (A) Schematic representation of plasmids used for production of HCVtcp. Deduced length of transcribed RNA from each construct is shown on the right. HCV polyproteins from JFH-1 strain are indicated by open boxes. HCV UTRs are indicated by bold lines. The EMCV IRES is denoted by gray bars. Adaptive mutations are indicated by asterisks. F Luc: firefly luciferase gene; P: RNA polymerase I promoter; T: RNA polymerase I terminator. (B) Detection of NS5B and actin in Huh7.5.1 cells transfected with indicated plasmids at 4 day post-transfection. (C) Infectivity of culture supernatants from cells transfected with indicated replicon plasmids along with pCAGC-NS2/JFH1am at 4 day post-transfection.

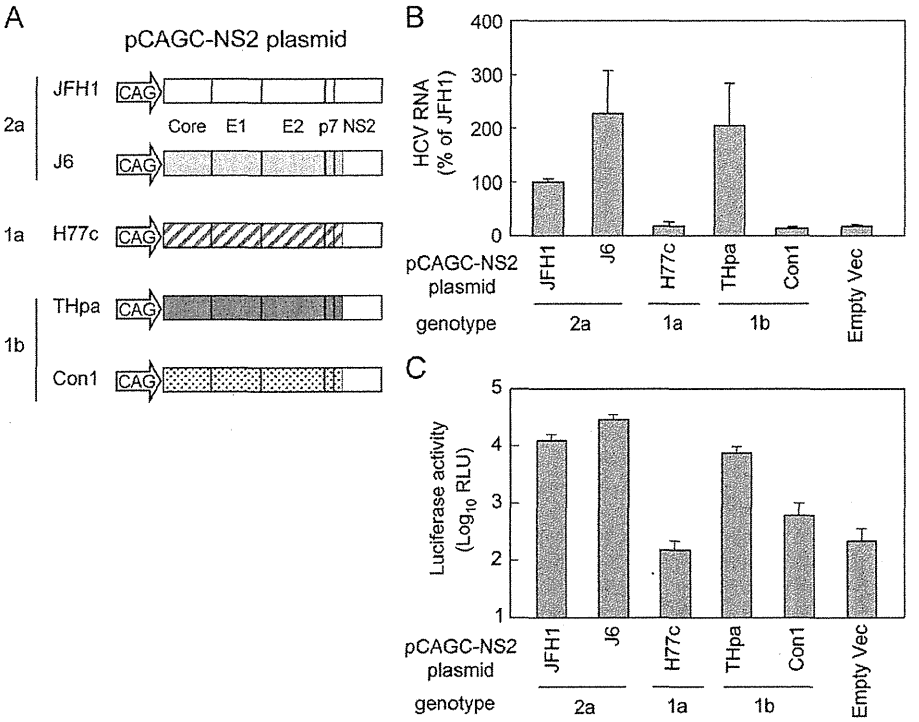

Fig. 3. HCVtcp production with structural proteins from various strains. (A) Schematic representation of plasmids used. HCV polyproteins of JFH-1, J6, H77c, THpa and Con1 strain are shown in the open box, bright gray box, box with diagonal lines, dark gray box and dotted box, respectively. (B) Relative levels of HCV RNA in the supernatant from cells transfected with indicated plasmids along with pHH/SGR-Luc. (C) Luciferase activity in cells inoculated with supernatant from cells transfected with indicated plasmids along with pHH/SGR-Luc at 4 day post-transfection.

pCAGC-NS2/THpa and pCAGC-NS2/JFH1am were used as core-NS2 plasmids for HCVtcp production carrying core-p7 derived from genotypes 1b and 2a (HCVtcp-1b and HCVtcp-2a, respectively). HCVpp derived from JFH-1 and VSVpp were generated and used for comparison. Infection with HCVtcp-1b or HCVtcp-2a was blocked by anti-ApoE antibody in a dose-dependent manner. In contrast, anti-ApoE antibody did not affect infection with HCVpp and VSVpp (Fig. 4A).

The CD81 dependence of infection was also compared between HCVtcp and HCVpp (Fig. 4B). Anti-CD81 antibody inhibited the entry of HCVtcp-1b, HCVtcp-2a, and HCVpp in a dose-dependent manner. The antibody had no effect on VSVpp infection. HCVtcp infection appears to be more sensitive to anti-CD81 antibody when compared with HCVpp infection; more than 60% inhibition was observed at 0.08 μg/mL anti-CD81 antibody for HCVtcp-1b and HCVtcp-2a, whereas approximately 50% inhibition was observed for HCVpp at 2 μg/mL antibody. Neutralization of HCVcc by anti-ApoE and anti-CD81 antibodies was also determined. Antibodies blocked HCVcc infection (Fig. 4C and D), as observed with HCVtcp. These results suggest that ApoE, as well as CD81, play an important role in HCVtcp infection. Thus, HCVtcp may be more useful for evaluating the HCV entry process than HCVpp.

Identification of novel culture-adaptive mutation in NS3 by serial passage of HCVtcp in packaging cells

The HCVtcp system was further applied to analyses of genetic changes during serial passages in target cells. As an initial attempt, supernatants of cells co-transfected with pCAGC-NS2/JFH1am and pHH/SGR were inoculated into Huh7.5.1 cells transiently transfected with pCAGC-NS2/JFH1am. However, infectious titer was lost after repeated inoculation, likely due to low HCVtcp titers and low efficiency of plasmid transduction (data not shown). To overcome this, we utilized recombinant adenovirus vectors (rAdVs) to provide core-NS2. As we were not able to obtain rAdV directly expressing core-NS2, conditional transgene expression based on a Cre-loxP strategy was employed (Kanegae et al., 1995). We constructed an rAdV containing core-NS2 gene downstream of a stuffer DNA flanked by a pair of loxP sites (AxCALNLH-CNS2). When cells were doubly infected with AxCALNLH-CNS2 and the Cre-expressing rAdV, AxCANCre (Kanegae et al., 1995), the Cre-mediated excisional deletion removed the stuffer DNA, resulting in core-NS2 expression under control of the CAG promoter (Fig. 5A). As expected, tightly regulated production of HCVtcp was observed. The cells infected with AxCANCre and AxCALNLH-CNS2 along with transduction of pHH/SGR-Luc produced HCVtcp at high levels. Production of HCVtcp was undetectable when either AxCANCre or AxCALNLH-CNS2 was not infected (Fig. 5B). The Cre-mediated rAdV expression system appears to have yielded considerably higher production of HCVtcp when compared with the settings for plasmid co-transfection.

Supernatants from cells in which core-NS2 was expressed using rAdVs and the subgenomic RNA derived from pHH/SGR replicated were inoculated into cells infected with AxCALNLH-CNS2 and AxCANCre (Fig. 6A). Blind passage was performed by sequentially transferring culture supernatants to cells infected with the above rAdVs. The two independent 10 blind passages (p10) showed virus titers of $> 1 \times 10^6$ IU/mL, which were markedly higher than those of the passage 0 (p0) stock cultures (4×10^4 IU/mL). Side-by-side infection analysis revealed that the HCVtcp p10 #1 achieved a virus titer approximately 36 times higher than that of HCVtcp p0 on the packaging cells at 6 day post-infection (Fig. 6B). Sequencing of the entire replicon in the supernatants at p10 in two independent experiments revealed

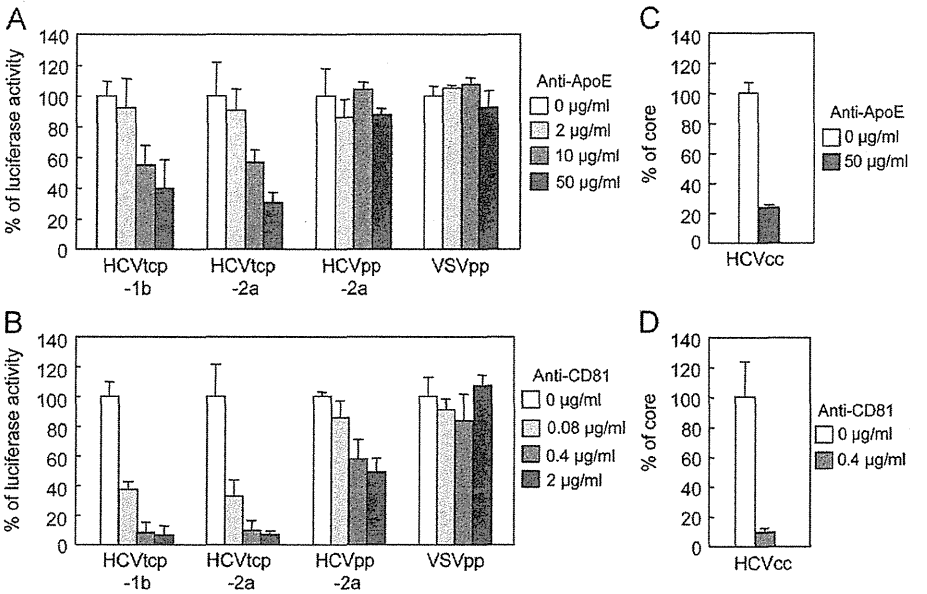

Fig. 4. Effects of anti-ApoE and anti-CD81 antibodies on HCV entry. (A) Aliquots of virus sample were incubated with increasing concentrations of anti-ApoE antibodies for 1 h and were then added to Huh7.5.1 cells. Luciferase activity was determined at 72 h post-infection and is expressed relative to activity without antibodies (white bar). (B) Huh7.5.1 cells were preincubated for 1 h with increasing concentrations of anti-CD81 antibodies, followed by inoculating virus samples. Luciferase activity was determined and expressed as shown in (A). (C) Aliquots of HCVcc were incubated with anti-ApoE antibodies for 1 h and were then added to Huh7.5.1 cells at an MOI of 0.05. Intracellular core levels were quantitated at 24 h post-infection and are expressed relative to levels without antibodies (white bar). (D) Huh7.5.1 cells were preincubated for 1 h with anti-CD81 antibodies. HCVcc infection and measurement of core proteins were performed as indicated in (C).

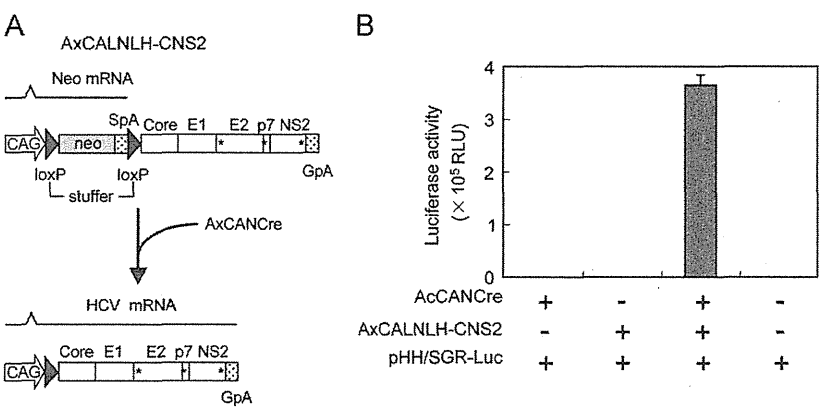

Fig. 5. Transgene activation mediated by rAdVs expressing Cre recombinase under control of CAG promoter. (A) Cre recobminase expressed by AxCANCre recognizes a pair of its target sequences loxP in AxCALNLH-CNS2, and removes the stuffer region resulting in expression of HCV core-NS2 polyprotein by CAG promoter. CAG: CAG promoter; SpA: SV40 early polyA signal; GpA: rabbit b-globin poly(A) signal. (B) Luciferase activity in Huh7.5.1 cells inoculated with 4-day post-transfection culture supernatant from cells transfected with pHH/SGR-Luc, and then infected with indicated rAdVs.

that both passaged HCVtcp had an identical nonsynonymous mutation in the NS3 region (N1586D) (Fig. 6C).

In order to examine the role of NS3 mutation identified on HCV RNA replication and on HCVtcp production, the N1586D mutation was introduced into pHH/SGR-Luc. Luciferase activities of the N1586D-mutated replicon were apparently lower than those of the WT-replicon, thus suggesting that the NS3 mutation reduced viral RNA replication (Fig. 7A). HCV RNA levels in the supernatants of cells transfected with WT- or mutant replicon plasmid along with pCAGC-NS2/JFH1am and luciferase activity in cells inoculated with supernatants from the transfected cells were then determined (Fig. 7B). The viral RNA level secreted from cells replicating the N1586D-mutated replicon was lower than that from cells replicating WT replicon (Fig. 7B, left). By contrast, a significantly higher infectivity of HCVtcp produced from the mutant replicon-cells was observed, as compared to WT replicon-cells (Fig. 7B, right), suggesting that the adaptive mutation increased the specific infectivity (almost 9-fold) of the virus particles. To further determine whether the N1586D mutation affects infectious viral assembly and/or virus release, we used the CD81-negative Huh-7 subclone, Huh7-25 (Akazawa et al., 2007), which may produce infectious particles, but is not susceptible to HCV entry due to a lack of CD81 expression, therefore allowing us to examine viral assembly and release without the influence of reinfection by produced HCVtcp. Measurement of intracellular and extracellular HCVtcp indicated that Huh7-25 cells replicating the N1586D-mutated replicon produced more infectious virus than WT in both supernatants and cell lysates (Fig. 7C). Thus, it can be concluded that the N1586D mutation contributes to enhanced infectious viral assembly, not RNA replication. We could not exclude the possibility that N1586D mutation affects virus release, since the mutation enhanced extracellular virus titers more than did the intracellular titer.

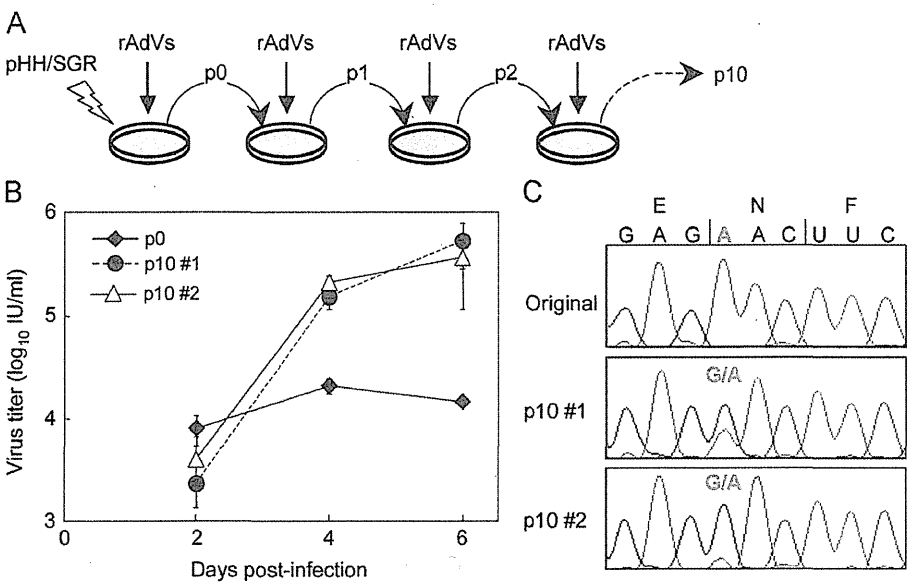

Fig. 6. Genotypic changes in HCVtcp following blind passage. (A) Experimental procedure for blind passage of HCVtcp. Huh7.5.1 cells were transfected with pHH/SGR and were doubly infected with AxCANCre and AxCALNLH-CNS2. Culture fluids were collected and were inoculated into cells infected with AxCANCre and AxCALNLH-CNS2. These procedures were repeated 10 times with two independent samples (#1 and #2). (B) Growth curves of HCVtcp p0 and p10 on Huh7.5.1 cells expressing core-NS2. Cells were infected with HCVtcp at an MOI of 0.05, and medium was collected at the indicated time points and subjected to titration. (C) Nucleotide sequences of original and blind-passaged replicons from HCVtcp. Nucleotides of mutated position are shown in red and bold.

The impact of the N1586D mutation on production of intra- and intergenotypic HCVtcp chimeras was also investigated. The N1586D mutation in the replicon enhanced the production of chimeric HCVtcp by providing core-p7 from all strains examined, although not statistically significant in THpa, and Con1 strains (Fig. 7D). Finally, to determine whether the N1586D mutation was responsible for enhancing HCVcc production, this mutation was introduced into pHHJFH1, which carries the full-length wild-type JFH-1 cDNA (Masaki et al., 2010), yielding pHHJFH1N1586D. The virus titer obtained from cells transfected with the pHHJFH1N1586D was significantly higher than that of WT (Fig. 7E), thus demonstrating that the N1586D mutation enhances yields of HCVcc, in addition to HCVtcp.

Discussion

Single-round infectious viral particles generated by *trans*-packaging systems are considered to be valuable tools for studying virus life cycles, particularly the steps related to entry into target cells, assembly and release of infectious particles. However, limited HCV strains have been applied for the efficient production of HCVtcp to date. In this study, we improved the HCVtcp system in order to enhance the productivity of infectious particles. Production of chimeric HCVtcp by providing genotype 1b-derived core-p7, in addition to intragenotypic viral proteins, was also confirmed. Furthermore, we exploited the system to investigate genetic changes during serial passage of target cells and identified a novel cell culture-adaptive mutation in NS3, which also contributes to enhance the productivity of HCVtcp.

HCVpp (Bartosch et al., 2003a; Hsu et al., 2003) has proven to be a valuable surrogate system by which the study of viral and cellular determinants of the viral entry pathway is possible. Early steps of HCV infection, including the role of HCV glycoprotein heterodimers, receptor binding, internalization and pH-dependent endosomal fusion, have been at least in part mimicked by HCVpp (Lavie et al., 2007). However, as HCVpp is generated in non-hepatic cells such as the human embryo kidney cells 293T, it is likely that the cell-derived component(s) of HCVpp differ from those of HCVcc. Hepatocytes play a role in maintaining lipid homeostasis in the body by assembling and secreting lipoproteins, including VLDL. It is highly likely that HCV exploits lipid synthesis pathways, as there is a tight link between virion formation and VLDL synthesis. Down-regulation of ApoE considerably reduces HCV production (Benga et al., 2010; Chang et al., 2007; Hishiki et al., 2010; Jiang and Luo, 2009; Owen et al., 2009). Infectivity of HCVcc is also neutralized by anti-ApoE antibodies (Chang et al., 2007). These data suggest that ApoE is important for HCV infectivity. Furthermore, Niemann-Pick C1-like 1 (NPC1L1), involving cholesterol uptake receptor, was recently identified as a host factor for HCV entry (Sainz et al., 2012). Knockdown of NPC1L1 had no effect on the entry of HCVpp whereas HCVcc entry was impaired, possibly due to different cholesterol content of these particles. Here, we found that the anti-ApoE antibody neutralized infection by HCVtcp and HCVcc, but not by HCVpp (Fig. 4A and C), thus suggesting that biogenesis and/or secretion pathways of VLDL are involved in HCVtcp similarly to HCVcc, but not in HCVpp.

We also observed that infectivity of HCVtcp and HCVcc is more efficiently neutralized by the anti-CD81 antibody, as compared to that of HCVpp (Fig. 4B and D). It has recently been reported that E2 of HCVcc contained both high-mannose-type and complex-type glycans, whereas most of the glycans on HCVpp-associated E2 were complex-type, which is matured by Golgi enzymes (Vieyres et al., 2010). Mutational analysis of the N-linked glycosylation sites in E1/E2 demonstrated that several glycans on E2 may affect the sensitivity of HCVpp against antibody neutralization, as well as access of CD81 to its binding site on E2 (Helle et al., 2010). The differences in sensitivity between HCVtcp and HCVpp to neutralization by anti-CD81 antibody observed here may be due to differences in carbohydrate composition of HCV glycoproteins during expression and processing of E1/E2 in cells and morphogenesis of HCVtcp and HCVpp.

By analyzing the various replicons for *trans*-packaging, we observed the highest production of HCVtcp with replicons from pHH/SGR, which lacked sequences not essential for RNA

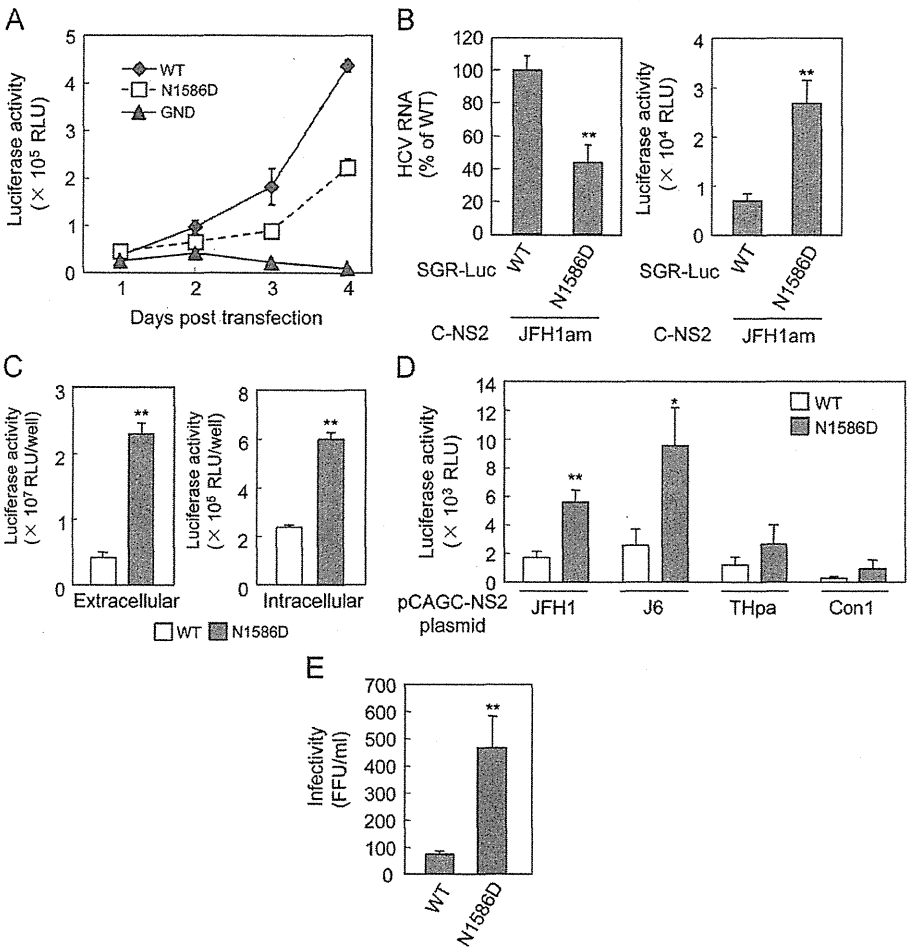

Fig. 7. Effects of N1586D mutation on RNA replication and production of HCVtcp or HCVcc. (A) RNA replication of replicons in cells transfected with pHH/SGR-Luc (WT) or N1586D mutant. Luciferase activities at 1 to 4 day post-transfection were determined. (B) Relative levels of HCV RNA in the supernatants from cells transfected with pHH/SGR-Luc (WT) or N1586D mutant plasmid along with pCAGC-NS2/JFH1am were shown in the left panel. Luciferase activities in cells inoculated with supernatants from cells transfected with indicated plasmids at 4 day post-transfection were shown in the right panel. (C) Luciferase activity in cells inoculated with supernatant and cell lysates from Huh7-25 cells transfected with pHH/SGR-Luc (WT) or N1586D mutant plasmid along with pCAGC-NS2/JFH1am at 5 day post-transfection. (D) Luciferase activity in cells inoculated with culture supernatant from cells transfected with pHH/SGR-Luc (WT) or N1586D mutant plasmid along with indicated core-NS2 plasmids at 4 day post-transfection. (E) Infectivity of supernatant from cells transfected with pHH/JFH1 (WT) or its derivative plasmid containing N1586D mutation at 6 day post-transfection. Statistical differences between WT and N1586D were evaluated using Student's *t*-test. $^{*}p < 0.05$, $^{**}p < 0.005$ vs. WT.

replication, while less efficient productivity was observed from pHH/SGR-Luc, pHH/SGR-C177, pHH/SGR-C191 and pHH/SGR-C-p7/am (Fig. 2C). Differences in the replication efficiency of the replicon do not appear to be a major determinant for HCVtcp productivity, at least in the present settings, as all replicon constructs except pHH/SGR-Luc replicated at similar levels, as confirmed by Western blotting (Fig. 2B). Although the shorter viral genome sequence may offer advantages over the longer sequence, further investigation is required in order to understand the molecular mechanisms underlying viral genome packaging. By comparing pHH/SGR vs. pHH/SGR-C177, pHH/SGR-C191 and pHH/SGR-C-p7/am, it is likely that the expression of the structural protein in *cis* does not increase HCVtcp production when sufficient amounts of structural proteins are supplied in *trans*.

Blind passage of HCVtcp in packaging cells infected with rAdVs providing core-NS2 enabled us to identify a novel culture-adaptive mutation in NS3. The N-terminal third of NS3 forms a serine protease, together with NS4A, and its C-terminal two-thirds exhibits RNA helicase and RNA-stimulated NTPase activities. In addition, similarly to flaviviruses (Kummerer and Rice, 2002; Liu et al., 2002), it is now apparent that HCV NS3 is also involved in viral morphogenesis (Han et al., 2009; Ma et al., 2008), although its precise role and underlying molecular mechanism(s) have not fully been elucidated. Two cell-culture adaptive NS3 mutations which are involved in HCV assembly have been identified. The Q1251L mutation in helicase subdomain 1 resulted in approximately 30-fold higher production of HCV without affecting NS3 enzymatic activities (Ma et al., 2008). The M1290K adaptive mutation was also located in subdomain 1 of the NS3 helicase (Han et al., 2009). The N1586D mutation identified here was located in subdomain 3 of helicase. Analogous to Q1251L and M1290K, the N1586D mutation enhanced the infectious viral assembly by increasing specific infectivity without affecting the efficiency of viral RNA replication. Considering the possibility that NS3 plays a role in linking between the viral replicase and assembly sites (Jones et al., 2011), it is likely that NS3 helicase is one of the determinants for interaction with the structural proteins. Our results, together with earlier studies, suggest that chimeric and defective mutations as well as supplying the viral components in *trans*, function as selective pressures in virion assembly.

In summary, we have established a plasmid-based reverse genetics for efficient production of HCVtcp with structural

proteins from various strains. Single-round infectious HCVtcp can complement the HCVcc and HCVpp systems as a valuable tool for the study of HCV life cycles.

Materials and methods

Cells

Huh7 derivative cell line Huh7.5.1 and Huh7-25 were maintained in Dulbecco modified Eagle medium (DMEM) supplemented with nonessential amino acids, 100 U of penicillin/mL, 100 μg of streptomycin/mL, and 10% fetal bovine serum at 37 °C in a 5% CO_2 incubator.

Plasmids

Plasmids pHHJFH1, pHH/SGR-Luc, pHH/SGR-Luc/GND and pCAG/C-NS2 were as described previously (Masaki et al., 2010). In this study, plasmid pCAG/C-NS2 was designated as pCAGC-NS2/JFH. The plasmid pCAGC-NS2/JFHam having adaptive mutations in E2 (N417S), p7 (N765D), and NS2 (Q1012R) in pCAGC-NS2/JFH was constructed by oligonucleotide-directed mutagenesis. These mutations were also introduced in pHHJFH1, resulting in pHHJFH1am. To generate core-NS2 expression plasmids with different strains of HCV, the cDNA coding core to the first transmembrane region of NS2 (33 amino acids) in pCAGC-NS2/JFH was replaced with the corresponding sequence of the J6 (Lindenbach et al., 2005), H77c (Yanagi et al., 1997), THpa (Shirakura et al., personal communication) and Con1 (Koch and Bartenschlager, 1999) strains. The THpa sequence contained the P to A mutation at 328 aa at E1 in the original TH strain. To generate pHH/SGR, pHH/SGR-Luc was digested with MluI and PmeI, followed by Klenow enzyme treatment and self-ligation to delete the luciferase coding sequence. To generate pHH/SGR-C177, pHH/SGR-C191 and pHH/SGR-C-p7/am, cDNA coding the partial core and luciferase in pHH/SGR-Luc were replaced with coding sequences for mature core (177aa), full-length core (191aa) or core-p7 polyprotein containing adaptive mutations in E2 and p7, respectively. The selected NS3 mutation (N1586D) was introduced into pHH/SGR-Luc and pHHJFH1 by oligonucleotide-directed mutagenesis.

Generation of viruses

HCVcc and HCVtcp were generated as described previously (Masaki et al., 2010). For the production of HCVpp-2a, plasmid pcDNAdeltaC-E1-E2(JFH1)am having adaptive mutations in E2 (N417S) in pcDNAdeltaC-E1-E2(JFH1) (Akazawa et al., 2007) was constructed by oligonucleotide-directed mutagenesis. Murine leukemia virus pseudotypes with VSV G glycoprotein expressing luciferase reporter (VSVpp) were generated in accordance with previously described methods (Akazawa et al., 2007; Bartosch et al., 2003a).

Luciferase assay

Huh7.5.1 cells were seeded onto a 24-well plate at a density of 3×10^4 cells/well 24 h prior to inoculation with reporter viruses. Cells were incubated for 72 h, followed by lysis with 100 μL of lysis buffer. Luciferase activity of the cells was determined using a luciferase assay system (Promega, Madison, WI). All luciferase assays were performed in triplicate.

Quantification of HCV infectivity and HCV RNA

To determine the titers of HCVtcp and HCVcc, Huh7.5.1 cell monolayers prepared in multi-well plates were incubated with dilutions of samples and then replaced with media containing 10% FBS and 0.8% carboxymethyl cellulose. Following incubation for 72 h, monolayers were fixed and immunostained with rabbit polyclonal anti-NS5A antibody, followed by Alexa Fluor 488-conjugated anti-rabbit secondary antibody (Invitrogen), and stained foci or individual cells were counted and used to calculate a titer of focus-forming units (FFU)/mL for spreading infections or infectious units (IU)/mL for non-spreading infections. For intracellular infectivity, the cell pellet was resuspended in culture media, and cells were lysed by four freeze–thaw cycles. Cell debris was pelleted by centrifugation for 5 min at 4000 rpm. Supernatant was collected and used for titration. To determine the amount of HCV RNA in culture supernatants, RNA was extracted from 140 μL of culture medium by QIAamp Viral RNA Mini Kit (QIAGEN, Valencia, CA) and treated with DNase (TURBO DNase; Ambion, Austin, TX) at 37 °C for 1 h. Extracted RNA was further purified by using an RNeasy Mini Kit, which includes RNase-free DNase digestion (QIAGEN). Copy numbers of HCV RNA were determined by real-time quantitative reverse transcription-PCR as described previously (Wakita et al., 2005).

Antibodies

Mouse monoclonal antibodies against actin (AC-15) and CD81 (JS-81) were obtained from Sigma (St. Louis, MO) and BD Biosciences (Franklin Lakes, NJ), respectively. Goat polyclonal antibody to ApoE (LV1479433) was obtained from Millipore (Tokyo, Japan). Anti-NS5A and anti-NS5B antibodies were rabbit polyclonal antibody against synthetic peptides.

Neutralization assay

For neutralization experiments with anti-CD81 antibody, Huh7.5.1 cells were incubated with dilutions of anti-CD81 antibody for 1 h at 37 °C. Cells were then infected with viruses for 5 h at 37 °C. For neutralization experiments with anti-ApoE antibody, viruses were incubated with various concentrations of anti-ApoE antibody at room temperature for 1 h and cells were infected with viruses for 5 h at 37 °C. Following infection, supernatant was removed and cells were incubated with culture medium, and luciferase activity was determined at 3 day post-infection for HCVtcp and pseudotyped viruses. For neutralization experiments with HCVcc generated with pHHJFH1am, a multiplicity of infection (MOI) of 0.05 was used for inoculation, and intracellular core protein levels were monitored by ELISA (Ortho Clinical Diagnostics) at 24 h post-infection.

Immunoblotting

Transfected cells were washed with PBS and incubated with lysis buffer (50 mM Tris–HCl, pH 7.4, 300 mM NaCl, 1% triton X-100). Lysates were then sonicated for 5 min and were added to the same volume of SDS sample buffer. Protein samples were boiled for 10 min, separated by SDS-PAGE, and transferred to PVDF membrane. After blocking, membranes were probed with first antibodies, followed by incubation with peroxidase-conjugated secondary antibody. Antigen–antibody complexes were visualized using an enhanced chemiluminescence detection system (Super Signal West Pico Chemiluminescent Substrate; PIERCE, Rockford, IL), in accordance with the manufacturer's protocols.

Generation of recombinant adenoviruses

rAdV, AxCANCre, expressing Cre recombinase tagged with nuclear localization signal under CAG promoter was prepared as described previously (Baba et al., 2005). The target rAdV AxCALNLH-CNS2 expressing HCV core-NS2 polyprotein with adaptive mutations in E2, p7 and NS2 was generated as follows. Cosmid pAxCALNLwit2 is identical to pAxCALNLw (Sato et al., 1998), except that both the terminal sequences of the rAdV genome are derived from pAxCAwit2 (Fukuda et al., 2006). The core-NS2 fragment obtained from pCAGC-NS2/JFH1am by StuI-EcoRI digestion and subsequent Klenow treatment was inserted into the SwaI site of pAxCALNLwit2. The resultant cosmid pAxCALNLH-CN2it2 was digested with PacI and transfected into 293 cells to generate rAdV AxCALNLH-CNS2.

Preparation of packaging cells for HCVtcp

Huh7.5.1 cells were coinfected with AxCANCre at an MOI of 1 and AxCALNLH-CNS2 at an MOI of 3 for expression of JFH-1 core-NS2 polyprotein containing the adaptive mutations in E2, p7 and NS2.

RNA preparation, RT-PCR and sequencing

Total cellular RNA was extracted with TRIzol reagent (Invitrogen, Carlsbad, CA), and subjected to reverse transcription with random hexamer and Superscript III reverse transcriptase (Invitrogen). Three fragments of HCV cDNAs that cover the entire HCV subgenomic replicon genome, were amplified by nested PCR with TaKaRa Ex Taq polymerase (Takara, Shiga, Japan). Amplified products were separated by agarose gel electrophoresis, and were used for direct DNA sequencing.

Acknowledgments

We are grateful to Francis V. Chisari (The Scripps Research Institute) for providing Huh7.5.1 cells. We thank M. Sasaki, M. Matsuda, and T. Date for their technical assistance, and T. Mizoguchi for the secretarial work. We also thank T. Masaki for their helpful discussions. This work was supported in part by grants-in-aid from the Ministry of Health, Labor, and Welfare and the Ministry of Education, Culture, Sports, Science, and Technology, Japan.

References

Adair, R., Patel, A.H., Corless, L., Griffin, S., Rowlands, D.J., McCormick, C.J., 2009. Expression of hepatitis C virus (HCV) structural proteins in trans facilitates encapsidation and transmission of HCV subgenomic RNA. J. Gen. Virol. 90 (Part 4), 833–842.

Akazawa, D., Date, T., Morikawa, K., Murayama, A., Miyamoto, M., Kaga, M., Barth, H., Baumert, T.F., Dubuisson, J., Wakita, T., 2007. CD81 expression is important for the permissiveness of Huh7 cell clones for heterogeneous hepatitis C virus infection. J. Virol. 81 (10), 5036–5045.

Baba, Y., Nakano, M., Yamada, Y., Saito, I., Kanegae, Y., 2005. Practical range of effective dose for Cre recombinase-expressing recombinant adenovirus without cell toxicity in mammalian cells. Microbiol. Immunol. 49 (6), 559–570.

Bartosch, B., Dubuisson, J., Cosset, F.L., 2003a. Infectious hepatitis C virus pseudoparticles containing functional E1-E2 envelope protein complexes. J. Exp. Med. 197 (5), 633–642.

Bartosch, B., Vitelli, A., Granier, C., Goujon, C., Dubuisson, J., Pascale, S., Scarselli, E., Cortese, R., Nicosia, A., Cosset, F.L., 2003b. Cell entry of hepatitis C virus requires a set of co-receptors that include the CD81 tetraspanin and the SR-B1 scavenger receptor. J. Biol. Chem. 278 (43), 41624–41630.

Benedicto, I., Molina-Jimenez, F., Bartosch, B., Cosset, F.L., Lavillette, D., Prieto, J., Moreno-Otero, R., Valenzuela-Fernandez, A., Aldabe, R., Lopez-Cabrera, M., Majano, P.L., 2009. The tight junction-associated protein occludin is required for a postbinding step in hepatitis C virus entry and infection. J. Virol. 83 (16), 8012–8020.

Benga, W.J., Krieger, S.E., Dimitrova, M., Zeisel, M.B., Parnot, M., Lupberger, J., Hildt, E., Luo, G., McLauchlan, J., Baumert, T.F., Schuster, C., 2010. Apolipoprotein E interacts with hepatitis C virus nonstructural protein 5A and determines assembly of infectious particles. Hepatology 51 (1), 43–53.

Chang, K.S., Jiang, J., Cai, Z., Luo, G., 2007. Human apolipoprotein E is required for infectivity and production of hepatitis C virus in cell culture. J. Virol. 81 (24), 13783–13793.

Cormier, E.G., Tsamis, F., Kajumo, F., Durso, R.J., Gardner, J.P., Dragic, T., 2004. CD81 is an entry coreceptor for hepatitis C virus. Proc. Natl. Acad. Sci. USA 101 (19), 7270–7274.

Evans, M.J., von Hahn, T., Tscherne, D.M., Syder, A.J., Panis, M., Wolk, B., Hatziioannou, T., McKeating, J.A., Bieniasz, P.D., Rice, C.M., 2007. Claudin-1 is a hepatitis C virus co-receptor required for a late step in entry. Nature 446 (7137), 801–805.

Flint, M., von Hahn, T., Zhang, J., Farquhar, M., Jones, C.T., Balfe, P., Rice, C.M., McKeating, J.A., 2006. Diverse CD81 proteins support hepatitis C virus infection. J. Virol. 80 (22), 11331–11342.

Fukuda, H., Terashima, M., Koshikawa, M., Kanegae, Y., Saito, I., 2006. Possible mechanism of adenovirus generation from a cloned viral genome tagged with nucleotides at its ends. Microbiol. Immunol. 50 (8), 643–654.

Han, Q., Xu, C., Wu, C., Zhu, W., Yang, R., Chen, X., 2009. Compensatory mutations in NS3 and NS5A proteins enhance the virus production capability of hepatitis C reporter virus. Virus Res. 145 (1), 63–73.

Helle, F., Vieyres, G., Elkrief, L., Popescu, C.I., Wychowski, C., Descamps, V., Castelain, S., Roingeard, P., Duverlie, G., Dubuisson, J., 2010. Role of N-linked glycans in the functions of hepatitis C virus envelope proteins incorporated into infectious virions. J. Virol. 84 (22), 11905–11915.

Hishiki, T., Shimizu, Y., Tobita, R., Sugiyama, K., Ogawa, K., Funami, K., Ohsaki, Y., Fujimoto, T., Takaku, H., Wakita, T., Baumert, T.F., Miyanari, Y., Shimotohno, K., 2010. Infectivity of hepatitis C virus is influenced by association with apolipoprotein E isoforms. J. Virol. 84 (22), 12048–12057.

Hoofnagle, J.H., 2002. Course and outcome of hepatitis C. Hepatology 36 (5 Suppl. 1), S21–9.

Hsu, M., Zhang, J., Flint, M., Logvinoff, C., Cheng-Mayer, C., Rice, C.M., McKeating, J.A., 2003. Hepatitis C virus glycoproteins mediate pH-dependent cell entry of pseudotyped retroviral particles. Proc. Natl. Acad. Sci. USA 100 (12), 7271–7276.

Ishii, K., Murakami, K., Hmwe, S.S., Zhang, B., Li, J., Shirakura, M., Morikawa, K., Suzuki, R., Miyamura, T., Wakita, T., Suzuki, T., 2008. Trans-encapsidation of hepatitis C virus subgenomic replicon RNA with viral structure proteins. Biochem. Biophys. Res. Commun. 371 (3), 446–450.

Jiang, J., Luo, G., 2009. Apolipoprotein E but not B is required for the formation of infectious hepatitis C virus particles. J. Virol. 83 (24), 12680–12691.

Jones, D.M., Atoom, A.M., Zhang, X., Kottilil, S., Russell, R.S., 2011. A genetic interaction between the core and NS3 proteins of hepatitis C virus is essential for production of infectious virus. J. Virol. 85 (23), 12351–12361.

Kanegae, Y., Lee, G., Sato, Y., Tanaka, M., Nakai, M., Sakaki, T., Sugano, S., Saito, I., 1995. Efficient gene activation in mammalian cells by using recombinant adenovirus expressing site-specific Cre recombinase. Nucl. Acids Res. 23 (19), 3816–3821.

Koch, J.O., Bartenschlager, R., 1999. Modulation of hepatitis C virus NS5A hyperphosphorylation by nonstructural proteins NS3, NS4A, and NS4B. J. Virol. 73 (9), 7138–7146.

Kummerer, B.M., Rice, C.M., 2002. Mutations in the yellow fever virus nonstructural protein NS2A selectively block production of infectious particles. J. Virol. 76 (10), 4773–4784.

Lavie, M., Goffard, A., Dubuisson, J., 2007. Assembly of a functional HCV glycoprotein heterodimer. Curr. Issues Mol. Biol. 9 (2), 71–86.

Lindenbach, B.D., Evans, M.J., Syder, A.J., Wolk, B., Tellinghuisen, T.L., Liu, C.C., Maruyama, T., Hynes, R.O., Burton, D.R., McKeating, J.A., Rice, C.M., 2005. Complete replication of hepatitis C virus in cell culture. Science 309 (5734), 623–626.

Liu, S., Yang, W., Shen, L., Turner, J.R., Coyne, C.B., Wang, T., 2009. Tight junction proteins claudin-1 and occludin control hepatitis C virus entry and are downregulated during infection to prevent superinfection. J. Virol. 83 (4), 2011–2014.

Liu, W.J., Sedlak, P.L., Kondratieva, N., Khromykh, A.A., 2002. Complementation analysis of the flavivirus Kunjin NS3 and NS5 proteins defines the minimal regions essential for formation of a replication complex and shows a requirement of NS3 in cis for virus assembly. J. Virol. 76 (21), 10766–10775.

Ma, Y., Yates, J., Liang, Y., Lemon, S.M., Yi, M., 2008. NS3 helicase domains involved in infectious intracellular hepatitis C virus particle assembly. J. Virol. 82 (15), 7624–7639.

Masaki, T., Suzuki, R., Saeed, M., Mori, K., Matsuda, M., Aizaki, H., Ishii, K., Maki, N., Miyamura, T., Matsuura, Y., Wakita, T., Suzuki, T., 2010. Production of infectious hepatitis C virus by using RNA polymerase I-mediated transcription. J. Virol. 84 (11), 5824–5835.

Mazumdar, B., Banerjee, A., Meyer, K., Ray, R., 2011. Hepatitis C virus E1 envelope glycoprotein interacts with apolipoproteins in facilitating entry into hepatocytes. Hepatology 54 (4), 1149–1156.

McKeating, J.A., Zhang, L.Q., Logvinoff, C., Flint, M., Zhang, J., Yu, J., Butera, D., Ho, D.D., Dustin, L.B., Rice, C.M., Balfe, P., 2004. Diverse hepatitis C virus glycoproteins mediate viral infection in a CD81-dependent manner. J. Virol. 78 (16), 8496–8505.

Owen, D.M., Huang, H., Ye, J., Gale Jr., M., 2009. Apolipoprotein E on hepatitis C virion facilitates infection through interaction with low-density lipoprotein receptor. Virology 394 (1), 99–108.

Pietschmann, T., Kaul, A., Koutsoudakis, G., Shavinskaya, A., Kallis, S., Steinmann, E., Abid, K., Negro, F., Dreux, M., Cosset, F.L., Bartenschlager, R., 2006. Construction and characterization of infectious intragenotypic and intergenotypic hepatitis C virus chimeras. Proc. Natl. Acad. Sci. USA 103 (19), 7408–7413.

Pileri, P., Uematsu, Y., Campagnoli, S., Galli, G., Falugi, F., Petracca, R., Weiner, A.J., Houghton, M., Rosa, D., Grandi, G., Abrignani, S., 1998. Binding of hepatitis C virus to CD81. Science 282 (5390), 938–941.

Ploss, A., Evans, M.J., Gaysinskaya, V.A., Panis, M., You, H., de Jong, Y.P., Rice, C.M., 2009. Human occludin is a hepatitis C virus entry factor required for infection of mouse cells. Nature 457 (7231), 882–886.

Russell, R.S., Meunier, J.C., Takikawa, S., Faulk, K., Engle, R.E., Bukh, J., Purcell, R.H., Emerson, S.U., 2008. Advantages of a single-cycle production assay to study cell culture-adaptive mutations of hepatitis C virus. Proc. Natl. Acad. Sci. USA 105 (11), 4370–4375.

Sainz Jr., B., Barretto, N., Martin, D.N., Hiraga, N., Imamura, M., Hussain, S., Marsh, K.A., Yu, X., Chayama, K., Alrefai, W.A., Uprichard, S.L., 2012. Identification of the Niemann-Pick C1-like 1 cholesterol absorption receptor as a new hepatitis C virus entry factor. Nat. Med. 18 (2), 281–285.

Sato, Y., Tanaka, K., Lee, G., Kanegae, Y., Sakai, Y., Kaneko, S., Nakabayashi, H., Tamaoki, T., Saito, I., 1998. Enhanced and specific gene expression via tissue-specific production of Cre recombinase using adenovirus vector. Biochem. Biophys. Res. Commun. 244 (2), 455–462.

Scarselli, E., Ansuini, H., Cerino, R., Roccasecca, R.M., Acali, S., Filocamo, G., Traboni, C., Nicosia, A., Cortese, R., Vitelli, A., 2002. The human scavenger receptor class B type I is a novel candidate receptor for the hepatitis C virus. EMBO J. 21 (19), 5017–5025.

Steinmann, E., Brohm, C., Kallis, S., Bartenschlager, R., Pietschmann, T., 2008. Efficient trans-encapsidation of hepatitis C virus RNAs into infectious virus-like particles. J. Virol. 82 (14), 7034–7046.

Suzuki, T., Ishii, K., Aizaki, H., Wakita, T., 2007. Hepatitis C viral life cycle. Adv. Drug Deliv. Rev. 59 (12), 1200–1212.

Tani, H., Komoda, Y., Matsuo, E., Suzuki, K., Hamamoto, I., Yamashita, T., Moriishi, K., Fujiyama, K., Kanto, T., Hayashi, N., Owsianka, A., Patel, A.H., Whitt, M.A., Matsuura, Y., 2007. Replication-competent recombinant vesicular stomatitis virus encoding hepatitis C virus envelope proteins. J. Virol. 81 (16), 8601–8612.

Vieyres, G., Thomas, X., Descamps, V., Duverlie, G., Patel, A.H., Dubuisson, J., 2010. Characterization of the envelope glycoproteins associated with infectious hepatitis C virus. J. Virol. 84 (19), 10159–10168.

Wakita, T., Pietschmann, T., Kato, T., Date, T., Miyamoto, M., Zhao, Z., Murthy, K., Habermann, A., Krausslich, H.G., Mizokami, M., Bartenschlager, R., Liang, T.J., 2005. Production of infectious hepatitis C virus in tissue culture from a cloned viral genome. Nat. Med. 11 (7), 791–796.

Yanagi, M., Purcell, R.H., Emerson, S.U., Bukh, J., 1997. Transcripts from a single full-length cDNA clone of hepatitis C virus are infectious when directly transfected into the liver of a chimpanzee. Proc. Natl. Acad. Sci. USA 94 (16), 8738–8743.

Zhong, J., Gastaminza, P., Cheng, G., Kapadia, S., Kato, T., Burton, D.R., Wieland, S.F., Uprichard, S.L., Wakita, T., Chisari, F.V., 2005. Robust hepatitis C virus infection in vitro. Proc. Natl. Acad. Sci. USA 102 (26), 9294–9299.

Immunity
Article

The Transcription Factor Jdp2 Controls Bone Homeostasis and Antibacterial Immunity by Regulating Osteoclast and Neutrophil Differentiation

Kenta Maruyama,[1] Masahiro Fukasaka,[1] Alexis Vandenbon,[2] Tatsuya Saitoh,[1] Takumi Kawasaki,[1] Takeshi Kondo,[1] Kazunari K. Yokoyama,[4] Hiroyasu Kidoya,[3] Nobuyuki Takakura,[3] Daron Standley,[2] Osamu Takeuchi,[1,5] and Shizuo Akira[1,3,*]

[1]Laboratory of Host Defense
[2]Laboratoy of Systems Immunology, WPI Immunology Frontier Research Center (IFReC)
[3]Research Institute for Microbial Diseases
Osaka University, Osaka 565-0871, Japan
[4]Cancer Center, Kaohsiung Medical University Hospital, 807 Kaohsiung, Taiwan
[5]Laboratory of Infection and Prevention, Institute for Virus Research, Kyoto University, Kyoto 606-8507, Japan
*Correspondence: sakira@biken.osaka-u.ac.jp
http://dx.doi.org/10.1016/j.immuni.2012.08.022

SUMMARY

Jdp2 is an AP-1 family transcription factor that regulates the epigenetic status of histones. Previous in vitro studies revealed that Jdp2 is involved in osteoclastogenesis. However, the roles of Jdp2 in vivo and its pleiotropic functions are largely unknown. Here we generated *Jdp2*$^{-/-}$ mice and discovered its crucial roles not only in bone metabolism but also in differentiation of neutrophils. *Jdp2*$^{-/-}$ mice exhibited osteopetrosis resulting from impaired osteoclastogenesis. *Jdp2*$^{-/-}$ neutrophils were morphologically normal but had impaired surface expression of Ly6G, bactericidal function, and apoptosis. We also found that ATF3 was an inhibitor of neutrophil differentiation and that Jdp2 directly suppresses its expression via inhibition of histone acetylation. Strikingly, *Jdp2*$^{-/-}$ mice were highly susceptible to *Staphylococcus aureus* and *Candida albicans* infection. Thus, Jdp2 plays pivotal roles in in vivo bone homeostasis and host defense by regulating osteoclast and neutrophil differentiation.

INTRODUCTION

Jun dimerization protein 2 (Jdp2) is a member of the AP-1 family and interacts with other AP-1 components, such as c-Jun, JunB, JunD, and ATF2 (Aronheim et al., 1997). Jdp2 can inhibit the activation of its binding partners, suggesting that it is a transcriptional repressor (Jin et al., 2001). Furthermore, Jdp2 suppresses histone acetyltransferase activity and acetylation of reconstituted nucleosomes, thereby regulating the epigenetic status of histones (Jin et al., 2006). Extensive studies have revealed that Jdp2 plays roles in various cellular responses, such as UV-induced apoptosis and osteoclastogenesis (Huang et al., 2010).

Osteoclasts are multinucleated cells that degrade bone (Karsenty and Wagner, 2002). Bone-forming osteoblasts express macrophage colony-stimulating factor (M-CSF) and RANK ligand (RANKL). When these cytokines stimulate their receptors, c-fms and RANK, respectively, transcription factors such as c-Fos, NF-κB, and NFATc1 (Takayanagi, 2007) are activated in osteoclast precursors and osteoclastogenesis is induced by stimulation of osteoclastogenic genes, such as tartrate-resistant acid phosphatase (TRAP) and cathepsin K (CTSK). Jdp2 was previously implicated in positive regulation of osteoclastogenesis via activation of the TRAP and CTSK promoters (Kawaida et al., 2003). Recent findings indicate that the Jdp2 locus is hypomethylated and that its transcript is upregulated in common myeloid precursors and granulocyte-macrophage progenitors relative to lymphoid lineages (Ji et al., 2010), suggesting that Jdp2 may also contribute to the differentiation of myeloid cells, such as neutrophils.

Neutrophils are critical for bacterial clearance. One of the most impressive morphological features of mature neutrophils is cytosolic granules, and the mRNA expressions of granule content genes are significantly higher in immature neutrophils than in mature neutrophils (Borregaard and Cowland, 1997; Borregaard et al., 2007). There are three different granule subtypes, i.e., primary, secondary, and tertiary, and the granule proteins play pivotal roles in bacterial killing. The other bactericidal agents derived from neutrophils are reactive oxygen species (ROS), such as superoxide (Forman and Thomas, 1986). Recently, a novel mechanism of bacterial and fungal killing mediated by chromatin structures was elucidated, termed the neutrophil extracellular trap (NET) (Brinkmann et al., 2004). This extracellular structure is released through a cell death requiring ROS production (Nishinaka et al., 2011) and chromatin decondensation (Li et al., 2010). Collectively, these findings demonstrate that neutrophils exert bactericidal activity through several complex machineries.

Generally, neutrophil subtypes can be distinguished by their surface markers CD11b and Ly6G. CD11b^{+}Ly6G^{lo} cells are immature neutrophils with a round nucleus, such as myelocytes, whereas CD11b^{+}Ly6G^{hi} cells are band-segmented mature neutrophils (Hestdal et al., 1991). By using such morphological and molecular cues, several studies have shown that various cytokines and transcription factors are critical for proper

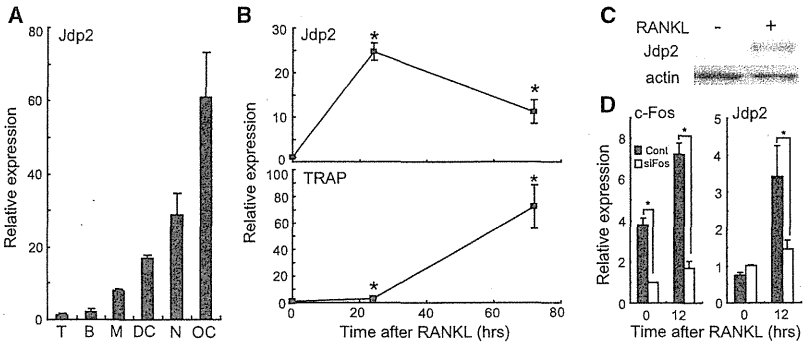

Figure 1. Jdp2 Expression
(A) qPCR analysis of Jdp2 in splenic T cells (T), B cells (B), DCs (DC), neutrophils (N), and primary bone marrow osteoclasts (OC) (n = 3).
(B) qPCR analysis of Jdp2 in MDMs in response to RANKL stimulation. *p < 0.05 versus 0 hr (n = 3).
(C) MDMs were stimulated with 50 ng/ml RANKL for 30 hr. Jdp2 levels were analyzed by protein immunoblotting.
(D) MDMs were transfected with control siRNA (Cont) or c-Fos-specific siRNA (siFos) and stimulated with 50 ng/ml RANKL for 12 hr. c-Fos and Jdp2 levels were measured by qPCR (n = 3).
*p < 0.05 versus control siRNA. Error bars, SE.

development of neutrophils. For example, granulocyte colony-stimulating factor (G-CSF) plays a pivotal role in proliferation of neutrophil precursors via activation of STAT3 (Lieschke et al., 1994). The CCAAT/enhancer binding protein (C/EBP) family is also critically involved in neutrophil differentiation. In particular, C/EBPα is considered a master regulator of neutrophils because C/EBPα-deficient mice lack neutrophils (Zhang et al., 1998). C/EBPε is involved in proper neutrophil differentiation, because neutrophils from C/EBPε-deficient mice have abnormal respiratory burst activity and lack secondary and tertiary granules (Yamanaka et al., 1997). Recent reports have also implicated the transcription factors Gfi-1 (Hock et al., 2003) and Ikaros (Dumortier et al., 2003) in proper differentiation of neutrophils. Overall, these findings suggest that neutrophil differentiation is orchestrated by interplay among several transcription factors.

Despite its importance in in vitro osteoclastogenesis and several implications for its activity in myeloid lineage cells, the roles of Jdp2 in vivo and its pleiotropic functions are completely unknown. Here, we generated *Jdp2*$^{-/-}$ mice and discovered critical roles of Jdp2 not only in bone homeostasis but also in proper differentiation of neutrophils.

RESULTS

Jdp2$^{-/-}$ Mice Are Osteopetrotic because of Impaired Osteoclastogenesis

First, we examined Jdp2 expression in mature myeloid cells, such as macrophages, dendritic cells (DCs), neutrophils, and osteoclasts. Jdp2 expression was substantially higher in these cells than in lymphoid cells, such as T and B cells (Figure 1A). Because Jdp2 expression was highest in osteoclasts (Figure 1A), we focused on the regulation of Jdp2 expression in response to RANKL. Jdp2 expression was significantly increased in M-CSF-derived macrophages (MDMs) after RANKL stimulation (Figures 1B and 1C) but not after LPS stimulation (Figure S1 available online). This transcriptional induction was dependent on c-Fos (based on siRNA knockdown), which is recognized as a pivotal transcription factor for osteoclastogenesis (Figure 1D). The existence of this c-Fos-Jdp2 axis prompted us to explore the role of Jdp2 in RANKL-induced osteoclastogenesis.

To evaluate osteoclastogenesis in vitro, *Jdp2*$^{-/-}$ mice were generated (Figures S2A–S2C). Surprisingly, in vitro RANKL-induced osteoclastogenesis and resorption pit formation were completely abrogated in *Jdp2*$^{-/-}$ cells (Figure 2A). We also evaluated the characteristics of splenic macrophages and found that the populations were similar between wild-type and *Jdp2*$^{-/-}$ cells (Figures S2D, S2E, and S2G). In addition, *Jdp2*$^{-/-}$ MDMs exhibited normal proliferation (Figure S2F) and RANK and c-fms expression (Figure S2H).

As previously reported (Kawaida et al., 2003), induction of osteoclast-associated genes, including TRAP and CTSK, was abrogated in *Jdp2*$^{-/-}$ cells, whereas c-Fos induction was comparable between wild-type and *Jdp2*$^{-/-}$ cells (Figure 2B). We also found that induction of NFATc1 mRNA and DNA binding of NFATc1 to its promoter was partially suppressed in *Jdp2*$^{-/-}$ cells in response to RANKL (Figures S2I and S2J). In addition, Jdp2 had no effect on NFATc1 binding to its promoter region (Figure S2K). Furthermore, DNA binding of NF-κB p65 was normal (Figure S2L). The expression levels of Blimp1, a positive regulator of osteoclastogenesis (Nishikawa et al., 2010), and Blimp1 target genes, such as *Irf8* and *Bcl6*, were comparable (Figure S2M). RANKL-induced calcium oscillation was normal in *Jdp2*$^{-/-}$ cells (Figure S2N). Because TREM2 is required for osteoclast multinucleation (Humphrey et al., 2006), we examined the TREM2 expression levels in wild-type and *Jdp2*$^{-/-}$ MDMs but found no difference (Figure S2O). When TREM2 was stimulated by antibody, wild-type MDMs formed increased numbers of osteoclasts. In contrast, TREM2 stimulation had no effect on osteoclastogenesis of *Jdp2*$^{-/-}$ MDMs (Figures S2P and S2Q). Finally, retrovirus reconstitution of Jdp2 in *Jdp2*$^{-/-}$ MDMs rescued RANKL-induced osteoclastogenesis (Figures S2R and S2S). Together, these results indicate that the c-Fos-Jdp2 axis is critical for controlling osteoclastogenesis via proper induction of NFATc1 and osteoclastogenic genes, such as *TRAP* and *CTSK*.

These findings prompted us to explore the role of Jdp2 in in vivo bone homeostasis. No apparent abnormalities were observed in *Jdp2*$^{-/-}$ mice, although they did exhibit slightly shortened femurs (Figure 2D). Radiographic analysis of the femurs showed that *Jdp2*$^{-/-}$ mice had osteopetrosis accompanied by marked increases in trabecular bone volume and number, compared with wild-type mice (Figures 2C, 2F, and 2G). These findings were further supported by increased bone mineral density (BMD) in the full-length femurs of *Jdp2*$^{-/-}$ mice (Figure 2E). Sections of proximal tibias from *Jdp2*$^{-/-}$ mice also showed increased trabecular bone volume and number (Figures 2H and 2I). Histomorphometric analysis revealed

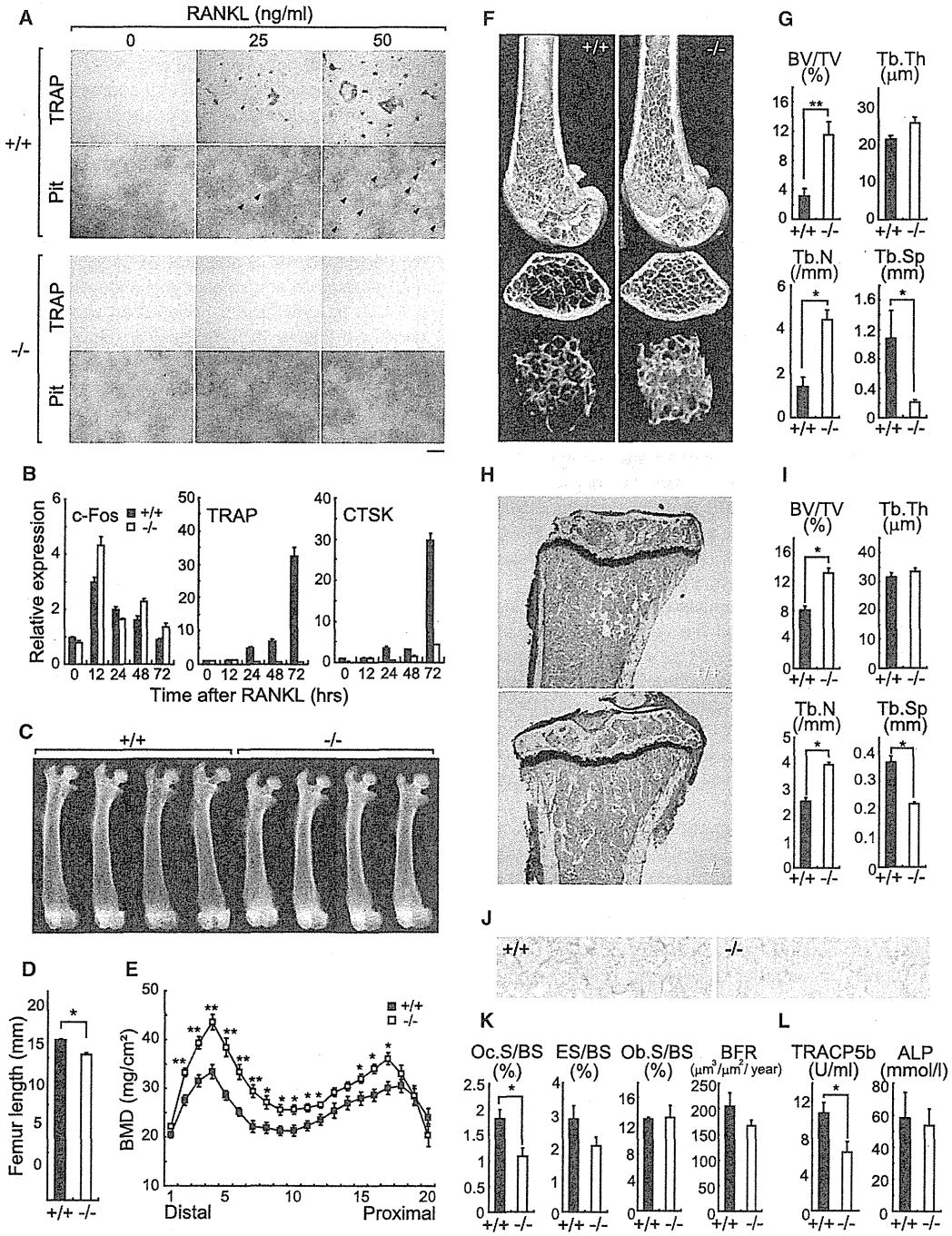

Figure 2. Impaired Osteoclastogenesis in *Jdp2*$^{-/-}$ Mice

(A) MDMs from wild-type and *Jdp2*$^{-/-}$ mice were cultured with the indicated concentrations of RANKL. Representative TRAP staining and resorption pits (arrowheads) are shown. Scale bar represents 200 μm.

(B) qPCR analysis of c-Fos, TRAP, and CTSK in wild-type and *Jdp2*$^{-/-}$ MDMs stimulated with 50 ng/ml RANKL (n = 3).

(C) Soft X-ray images of femurs.

(D) Femur lengths.

(E) BMDs of 20 longitudinal femur divisions.

(F) Representative μCT images of distal femurs (top, longitudinal view; middle, axial view of metaphyseal region; bottom, 3D view of metaphyseal region).

(G) Bone morphometric analysis of distal femurs by μCT.

a significant reduction in the osteoclast surface/bone surface ratio in *Jdp2*$^{-/-}$ mice, whereas the osteoblast surface/bone surface ratio and bone formation rate were normal (Figures 2J and 2K). Consistent with the decreased osteoclastogenesis in vivo, the serum bone resorption marker TRACP5b was lower in *Jdp2*$^{-/-}$ mice (Figure 2L). Furthermore, wild-type mice engrafted with bone marrow cells from *Jdp2*$^{-/-}$ mice had an increased bone volume phenotype (Figures S2T and S2U). Collectively, these results indicate that Jdp2 is critical for controlling osteoclastogenesis both in vitro and in vivo.

Neutrophils in *Jdp2*$^{-/-}$ Mice Are Morphologically Normal but Show Impaired Ly6G Expression

A recent report suggested that Jdp2 may be involved in the choice between lymphoid or myeloid differentiation (Ji et al., 2010). Therefore, we focused on the populations of lymphoid and myeloid cells (Figure S3A). No differences in the expressions of cell surface phenotype markers and numbers and ratios of T cells, B cells, and DCs in the spleen were observed between wild-type and *Jdp2*$^{-/-}$ mice (Figure S3A). We also checked the cytokine production (Figures S3B and S3C), bactericidal function (Figure S3D), superoxide production (Figure S3E), and phagocytosis activity (Figure S3F) in *Jdp2*$^{-/-}$ MDMs and conventional DCs (cDCs), and all phenotypes were normal.

Because Jdp2 was highly expressed in mature splenic neutrophils (Figure 1A), we compared the Jdp2 mRNA and protein expression between splenic and bone marrow neutrophils. Jdp2 expression in bone marrow mature CD11b^{+}Ly6G^{hi} neutrophils was lower than that in splenic mature CD11b^{+}Ly6G^{hi} neutrophils, but higher than that in bone marrow immature CD11b^{+}Ly6G^{lo} neutrophils (Figures S3G and S3H). These findings suggest that Jdp2 gradually increases during neutrophil differentiation and maturation.

To check the maturity of neutrophils from *Jdp2*$^{-/-}$ mice, we performed FACS analyses by using CD11b and Ly6G markers (Figure 3A). In *Jdp2*$^{-/-}$ bone marrow cells, the proportion of the CD11b^{+}Ly6G^{hi} population was shifted toward the CD11b^{+} Ly6G^{lo} population (Figure 3A). This low level of Ly6G indicated accumulation of immature cells. However, contrary to our expectation, *Jdp2*$^{-/-}$ neutrophils displayed a normal segmented nuclear morphology (Figure 3A). Because the CD11b^{+} population includes a Ly6C^{hi}Ly6G^{lo} inflammatory monocyte population (Colonna et al., 2004; Lagasse and Weissman, 1996) and a Ly6C^{lo}Ly6G^{+} neutrophil population, CD11b^{+} cells were further gated on CD11b^{+}Ly6C^{lo}Ly6G^{+} neutrophils and CD11b^{+}Ly6C^{hi} Ly6G^{lo} inflammatory monocytes to exclude monocytes from the *Jdp2*$^{-/-}$ CD11b^{+}Ly6G^{+} population (Figure 3B). Among CD11b^{+}Ly6C^{lo}Ly6G^{+} neutrophil populations, the CD11b^{+}Ly6C^{lo} Ly6G^{hi} population was shifted to the CD11b^{+}Ly6C^{lo}Ly6G^{lo} population in *Jdp2*$^{-/-}$ mice (Figure 3B). In contrast, CD11b^{+} Ly6C^{hi}Ly6G^{lo} inflammatory monocyte populations were comparable between wild-type and *Jdp2*$^{-/-}$ cells (Figure 3B). We also confirmed that both wild-type and *Jdp2*$^{-/-}$ CD11b^{+}Ly6C^{lo}Ly6G^{+} neutrophil populations had similar segmented nuclei (Figure 3B).

To further assess the abnormal bone marrow CD11b^{+} Ly6C^{lo}Ly6G^{+} neutrophil population in *Jdp2*$^{-/-}$ mice, we analyzed the cellular microstructure by transmission electron microscopy (TEM) (Figure 3C). However, the intracellular morphology of *Jdp2*$^{-/-}$ cells seemed normal (Figure 3C). To determine whether the abnormal neutrophils accumulated only in the bone marrow, we performed FACS analyses of thioglycollate-elicited peritoneal neutrophils and splenocytes (Figures 3D and 3E). An atypical CD11b^{+}Ly6C^{lo}Ly6G^{lo} population was observed in *Jdp2*$^{-/-}$ peritoneal (Figure 3D) and splenic (Figure 3E) neutrophils. To determine whether the defect in neutrophils in *Jdp2*$^{-/-}$ mice was bone marrow derived and cell intrinsic, we engrafted irradiated wild-type mice with *Jdp2*$^{-/-}$ or wild-type bone marrow. After reconstitution, we observed the same phenotype of neutrophils in the wild-type mice with *Jdp2*$^{-/-}$ bone marrow as in the *Jdp2*$^{-/-}$ mice (Figures S3O–S3Q). Together, these findings suggest that *Jdp2*$^{-/-}$ neutrophils are morphologically normal but have diminished Ly6G expression and that this abnormality arises in a cell-intrinsic manner.

Impaired Apoptosis and Bactericidal Function in *Jdp2*$^{-/-}$ Neutrophils

Intriguingly, we observed slight increases in CD11b^{+}Ly6C^{lo} Ly6G^{+} neutrophil numbers (~20%) in *Jdp2*$^{-/-}$ bone marrow and peripheral populations (Figures 3A, 3B, and 3E). Given this observation, we examined the spontaneous apoptosis of *Jdp2*$^{-/-}$ peritoneal neutrophils (Figure 3F). To our surprise, *Jdp2*$^{-/-}$ neutrophils showed impaired apoptosis compared with wild-type neutrophils (Figure 3F). Microarray and quantitative PCR (qPCR) analyses of neutrophils revealed that Bcl-2 expression was significantly increased in *Jdp2*$^{-/-}$ neutrophils, whereas Jdp2 deficiency had no effect on the diverse array of other Bcl-2-associated genes (Figures 3G–3I). Next, several assays were used to examine *Jdp2*$^{-/-}$ peritoneal neutrophil function. First, the capacity of *Jdp2*$^{-/-}$ mice to recruit neutrophils into the peritoneal cavity after thioglycollate injection was determined, with no difference in cell numbers found between wild-type and *Jdp2*$^{-/-}$ mice (Figure S3I). Second, we checked the cytokine production by *Jdp2*$^{-/-}$ neutrophils and found that Jdp2 deficiency did not alter cytokine production in response to TLR ligands (Figure S3J). Third, we analyzed the function of Jdp2 in NET formation. Intriguingly, we observed a 50% reduction in NET formation in neutrophils from *Jdp2*$^{-/-}$ mice in response to *Staphylococcus aureus* and *Candida albicans* infection (Figures 3J–3M). Fourth, because ROS, such as superoxide, are required for NET formation, we quantified superoxide production by *Jdp2*$^{-/-}$ neutrophils in

(H) Representative proximal tibias.
(I) Bone morphometric analysis of proximal tibias.
(J) TRAP staining of metaphyseal portions of tibias.
(K) Bone histomorphometric analysis of metaphyseal portions of tibias.
(L) Serum levels of TRACP5b and alkaline phosphatase (ALP).
Abbreviations: BV/TV, bone volume per tissue volume; Tb.Th, trabecular bone thickness; Tb.N, trabecular bone number; Tb.Sp, trabecular bone spacing; Oc.S/BS, osteoclast surface per bone surface; ES/BS, eroded surface per bone surface; Ob.S/BS, osteoblast surface per bone surface; BFR, bone formation rate. Error bars, SE. *$p < 0.05$; **$p < 0.01$ ($n = 4$).

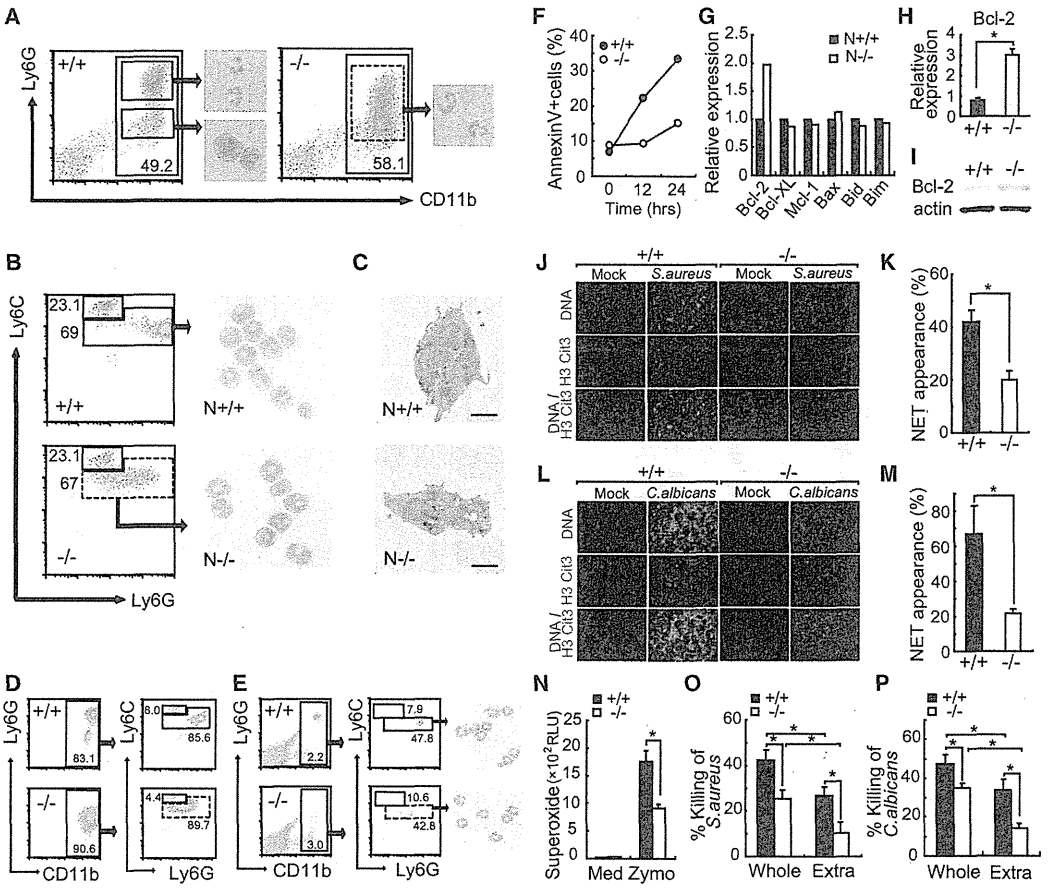

Figure 3. Abnormal Phenotype of *Jdp2*$^{-/-}$ Neutrophils

(A) FACS analysis of wild-type and *Jdp2*$^{-/-}$ bone marrow cells via Ly6G and CD11b markers. Gated cells were sorted and stained with May-Grunwald-Giemsa.

(B) CD11b^{+} populations in (A) were further analyzed with Ly6C marker. CD11b^{+}Ly6C^{lo}Ly6G^{+} neutrophils (N+/+ and N−/−) were sorted and stained as in (A).

(C) N+/+ and N−/− cells were fixed, stained with diaminobenzidine, and analyzed by TEM. Scale bars represent 2 μm.

(D and E) Peritoneal neutrophils (D) and splenocytes (E) were analyzed as in (B).

(F) Peritoneal neutrophils were cultured in vitro and analyzed for the percentage of annexin V-positive cells by FACS (n = 3 independent experiments).

(G) mRNA levels of apoptosis-regulating genes in bone marrow CD11b^{+}Ly6C^{lo}Ly6G^{+} neutrophils (N+/+ and N−/−) analyzed by a microarray.

(H and I) Bcl2 mRNA (H) and protein (I) expression levels in wild-type and *Jdp2*$^{-/-}$ peritoneal neutrophils were analyzed by qPCR and protein immunoblotting, respectively (n = 3).

(J) Peritoneal neutrophils were infected by *S. aureus* for 2 hr (MOI = 50) and stained by Hoechst and anti-histone H3 Cit3 Ab. DNA-histone H3 Cit3 Ab double-positive structures were defined as NETs.

(K) 50 microscopic fields (40×) in wells containing *S. aureus*-infected neutrophils, shown in (J), were checked and the rate of NET appearance was calculated (n = 4 observations).

(L) Peritoneal neutrophils were infected by *C. albicans* for 2 hr (MOI = 50) and stained as in (J).

(M) *C. albicans*-induced NET formation in (L) was measured as in (K).

(N) Peritoneal neutrophils were stimulated with 100 μg/ml Zymosan for 15 min and supernatant superoxide levels were measured.

(O) *S. aureus* killing by peritoneal neutrophils. Phagocytosis was inhibited by cytochalasin D and bacterial killing was measured (Extra) (n = 6).

(P) *C. albicans* killing by peritoneal neutrophils was determined as in (O).

Error bars, SE. *p < 0.05.

response to Zymosan and Curdlan. We observed 50% reductions in superoxide production in *Jdp2*$^{-/-}$ neutrophils (Figures 3N and S3L). We also checked the expression of Dectin-1, a Curdlan receptor, and observed similar expression levels between wild-type and *Jdp2*$^{-/-}$ neutrophils (Figure S3K). To clarify the mechanisms of decreased superoxide production in Jdp2 deficiency, we checked the expression levels of NADPH oxidase subunits and found that NCF1 expression was lower in *Jdp2*$^{-/-}$ neutrophils than in wild-type cells (Figure S3M). Therefore, we infected *Jdp2*$^{-/-}$ neutrophils with a retrovirus encoding NCF1 and measured the superoxide production. However, the rescue of *Jdp2*$^{-/-}$ neutrophils by NCF1 was less efficient than that by Jdp2 (Figure S3N). Thus, increased NCF1 can partially rescue the impaired superoxide production in *Jdp2*$^{-/-}$ neutrophils. Finally, to determine whether the functional defects of *Jdp2*$^{-/-}$ neutrophils were associated with bacterial killing

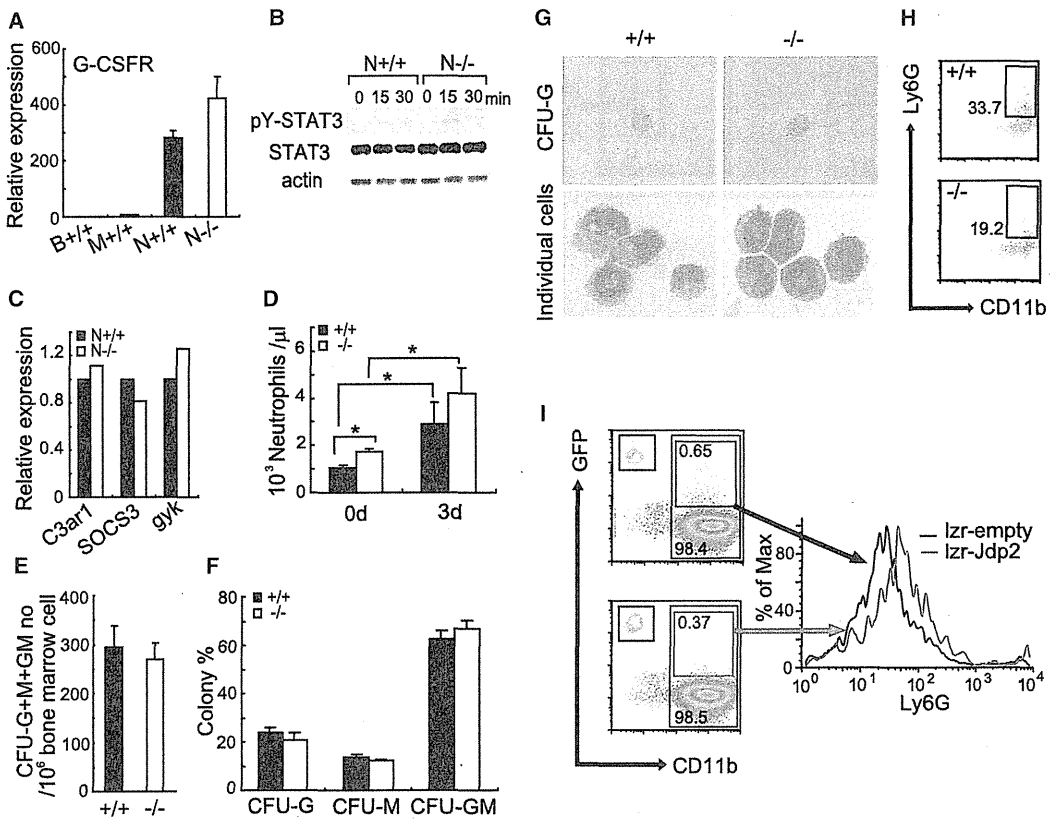

Figure 4. G-CSF Response Kinetics of *Jdp2*$^{-/-}$ Cells

(A) G-CSFR mRNA levels in wild-type and *Jdp2*$^{-/-}$ bone marrow CD11b^{+}Ly6C^{lo}Ly6G^{+} neutrophils (N+/+ and N−/−) measured by qPCR. Error bars, SE (n = 3).

(B) Cells in (A) were stimulated with 100 ng/ml G-CSF. STAT3 and pY-STAT3 levels were detected by immunoblotting.

(C) mRNA levels of STAT3 target genes in CD11b^{+}Ly6C^{lo}Ly6G^{+} neutrophils (N+/+ and N−/−) analyzed by a microarray.

(D) G-CSF (1 μg) was subcutaneously injected into wild-type and *Jdp2*$^{-/-}$ mice from days 0 to 3. At 6 hr after the last injection, blood was collected and CD11b^{+}Ly6G^{+} neutrophils were counted. Error bars, SE (n = 3). *p < 0.05.

(E and F) Bone marrow cells were cultured for 7 days in MethoCult. Total numbers of CFU-G, CFU-M, and CFU-GM colonies (E) and their rates (F) were determined. Error bars, SE (n = 6).

(G) Bone marrow cells were cultured for 7 days in MethoCult with 50 ng/ml G-CSF. Representative images of CFU-G and diaminobenzidine plus May-Grunwald-Giemsa-stained individual cells are indicated.

(H) CFU-G in (G) were collected and analyzed by FACS with CD11b and Ly6G markers.

(I) *Jdp2*$^{-/-}$ bone marrow cells were infected with a retrovirus encoding Jdp2 and GFP (Izr-Jdp2) or GFP alone (Izr-empty) with G-CSF for 9 days. CD11b^{+}GFP^{+} cells were gated and Ly6G expression levels were quantified by FACS. Gated cells were also sorted and stained by May-Grunwald-Giemsa (upper left insets in the scatter plots).

deficits, we performed in vitro killing assays with *S. aureus* and *C. albicans* (Figures 3O and 3P). Phagocytosis-dependent intracellular killing was inhibited by pretreating neutrophils with cytochalasin D. We observed that component killing mainly occurred in the extracellular space (Figures 3O and 3P) and that whole and extracellular bacterial killing by neutrophils from *Jdp2*$^{-/-}$ mice was significantly decreased compared with wild-type mice (Figures 3O and 3P). Together, these results clearly indicate that the bactericidal function is impaired in *Jdp2*$^{-/-}$ neutrophils.

Abnormal Differentiation of *Jdp2*$^{-/-}$ Neutrophils In Vitro Is Corrected by Re-expression of Jdp2

To investigate whether G-CSF signaling is altered by Jdp2 deficiency, we examined the expression levels of G-CSF receptor and STAT3. We found that G-CSF receptor (G-CSFR) expression was comparable between wild-type and *Jdp2*$^{-/-}$ neutrophils (Figure 4A), as was the expression of both STAT3 and phosphorylated STAT3 (Figure 4B). Microarray data confirmed the normal expression levels of G-CSF target genes (Figure 4C). We also counted the blood neutrophil numbers after intraperitoneal G-CSF injection and found comparable increasing rates of neutrophil numbers between wild-type and *Jdp2*$^{-/-}$ mice (Figure 4D). Thus, loss of Jdp2 does not influence G-CSF signaling.

Subsequently, we examined whether the altered differentiation of neutrophils in *Jdp2*$^{-/-}$ mice was a late-phase abnormality. *Jdp2*$^{-/-}$ bone marrow cells gave rise to the same numbers of granulocyte colony-forming units (CFU-G), granulocyte-macrophage colony-forming units (CFU-GM), and macrophage

colony-forming units (CFU-M) as did wild-type cells, with similar rates of formation (Figures 4E and 4F). We also added G-CSF to stem cell medium and cultured bone marrow cells (Figure 4G). As expected, the colony numbers (data not shown) and morphology (Figure 4G) between the two cell types were similar, but Ly6G expression was decreased in cells derived from *Jdp2*$^{-/-}$ bone marrow colonies (Figure 4H). Together, our findings imply that the abnormality in neutrophils from *Jdp2*$^{-/-}$ mice arises in the late differentiation phase and not in the initial differentiation phase.

Finally, we determined whether reintroduction of Jdp2 could rescue the terminal differentiation. We infected *Jdp2*$^{-/-}$ bone marrow cells with a retrovirus encoding Jdp2 and GFP or GFP alone and cultured the cells in medium containing G-CSF (Figure 4I). After 9 days, the cells were harvested and their Ly6G expression levels in gated GFP-positive neutrophils were quantified by FACS (Figure 4I). As expected, *Jdp2*$^{-/-}$ bone marrow-derived neutrophils infected with the Jdp2-GFP retrovirus exhibited increased Ly6G expression compared with control GFP-only cells (Figure 4I). Thus, the defect in neutrophil differentiation in *Jdp2*$^{-/-}$ mice appears to be cell autonomous and can be corrected by re-expression of Jdp2.

Primary Granule mRNA Expression Is Elevated in *Jdp2*$^{-/-}$ Neutrophils

The mRNA levels of granule genes are higher in immature neutrophils than in mature neutrophils (Martinelli et al., 2004). Therefore, we analyzed the diverse RNAs of CD11b^{+}Ly6C^{lo}Ly6G^{+} bone marrow neutrophils encoding primary, secondary, and tertiary granules by using microarray data (Figure 5A). Intriguingly, the mRNA levels for primary granule proteins, such as MPO, CTSG, and PR3, were significantly increased in *Jdp2*$^{-/-}$ neutrophils, whereas those for secondary and tertiary granule proteins were comparable to control cells (Figure 5A). The expression of other bactericidal granule proteins, such as Lipocalin2 and Cramp, was comparable (Figure S4A). We confirmed these aberrant primary granule expressions in bone marrow and peritoneal neutrophils by qPCR (Figures 5B and 5C). However, in immunoblotting analyses, the expression levels of primary granule proteins (Figure 5D) and their degranulation in response to LPS (Figure S4B) seemed comparable between wild-type and *Jdp2*$^{-/-}$ neutrophils.

To reveal the mechanism of the aberrant mRNA expression in *Jdp2*$^{-/-}$ neutrophils, we selected a set of genes whose expression levels were more abundant in *Jdp2*$^{-/-}$ neutrophils than in wild-type cells (Figure S4C) based on microarray data and examined their promoters for the presence of transcription factor binding sites. The analysis revealed that C/EBP binding sequences were highly enriched in the promoters of Jdp2-regulated genes compared with randomly selected gene promoters (Figures S4C–S4E). Further, we found that C/EBP binding sites were most enriched among 198 transcription factor binding sequences tested (Table S1). Thus, we quantified the mRNAs of the C/EBP gene family involved in myeloid differentiation. However, their expression levels were comparable (Figure 5E). C/EBPα was reported to be the master regulator of the expression of primary granule genes (Zhang et al., 1998). Therefore, we examined the DNA-binding activities of C/EBPα and C/EBPβ to their consensus oligonucleotides by using ELISA-based transcription factor kits (Figure 5F). Although the protein expression levels were again comparable (Figure 5G), C/EBPα, but not C/EBPβ, DNA binding was increased in *Jdp2*$^{-/-}$ neutrophils (Figure 5F). In addition, Jdp2 binding to the C/EBPα promoter was not detected by chromatin immunoprecipitation (ChIP) analyses (Figure 5H). When GFP-fused Jdp2 was retrovirally overexpressed in primary neutrophils, its expression was restricted to the nucleus (Figure S4F). These observations led us to examine the binding of Jdp2 to C/EBPα, and an association between C/EBPα and Jdp2 was found by immunoprecipitation (Figures 5I and 5J). From this, we examined the effect of Jdp2 on the transcriptional activity of C/EBPα (Figure 5K). For this experiment, we used a luciferase reporter plasmid driven by C/EBP transcriptional response elements. Overexpression of the C/EBPα gene only activated this promoter, whereas simultaneous expression of Jdp2 dose dependently reduced the activity of the promoter to the control level (Figure 5K). Together, these findings suggest that Jdp2 inhibits the transcriptional activity of C/EBPα by directly binding to the gene and inhibiting C/EBPα from binding to its target sequence. We also overexpressed C/EBPα in wild-type bone marrow cells and found that C/EBPα enhanced primary granule mRNAs (Figures S4G and S4H). Furthermore, when we re-expressed Jdp2 in *Jdp2*$^{-/-}$ bone marrow cells, DNA binding of C/EBPα and expression of primary granule genes were downregulated (Figures S4I and S4J). We also overexpressed C/EBPα in wild-type differentiated neutrophils (Figure S4K) and found that expression of Bcl-2 (Figure S4M) but not Ly6G (Figure S4L) was induced, leading to impaired apoptosis (Figure S4N). Together, our observations strengthen the idea that *Jdp2*$^{-/-}$ neutrophils are immature and suggest that increased primary granule and Bcl-2 mRNA expressions are attributable to increased C/EBPα activation.

ATF3 Is a Target of Jdp2 and Regulates Ly6G Expression

Among AP-1 family members, ATF3 is the closest relative of Jdp2 (Figure 6A). This information prompted us to measure ATF3 expression in neutrophils. ATF3 expression in bone marrow and peritoneal neutrophils was significantly increased (Figure 6B). We also overexpressed Jdp2 in wild-type and *Jdp2*$^{-/-}$ neutrophils and found that Jdp2 suppressed ATF3 expression (Figures 6C and 6D). Jdp2 is known to act as an epigenetic regulator of gene expression (Jin et al., 2006). Therefore, we analyzed the genome-wide status of histone acetylation, H3K4 trimethylation, and H3K27 trimethylation in wild-type and *Jdp2*$^{-/-}$ peritoneal neutrophils by using the ChIP-sequencing (ChIP-Seq) technique (Figure 6E). First, genes were chosen based on their differences in expression in wild-type and *Jdp2*$^{-/-}$ neutrophils. However, we did not find an apparent correlation between epigenetic statuses (data not shown). Moreover, primary granule genes did not have significant peaks for acetyl-histone, H3K4me3, and H3K27me3 in either wild-type or *Jdp2*$^{-/-}$ peritoneal neutrophils (Figure S5), indicating that expression of these genes is not regulated by the epigenetic status. When we focused on the ATF3 locus, we found a dramatic increase in the acetyl-histone status of the promoter region close to the transcription start site (Figure 6E). However, the same region had comparable H3K4me3 and H3K27me3 statuses (Figure 6E). By ChIP analyses, we confirmed an increase in the acetyl-histone status at the ATF3 promoter region in *Jdp2*$^{-/-}$ peritoneal neutrophils and observed

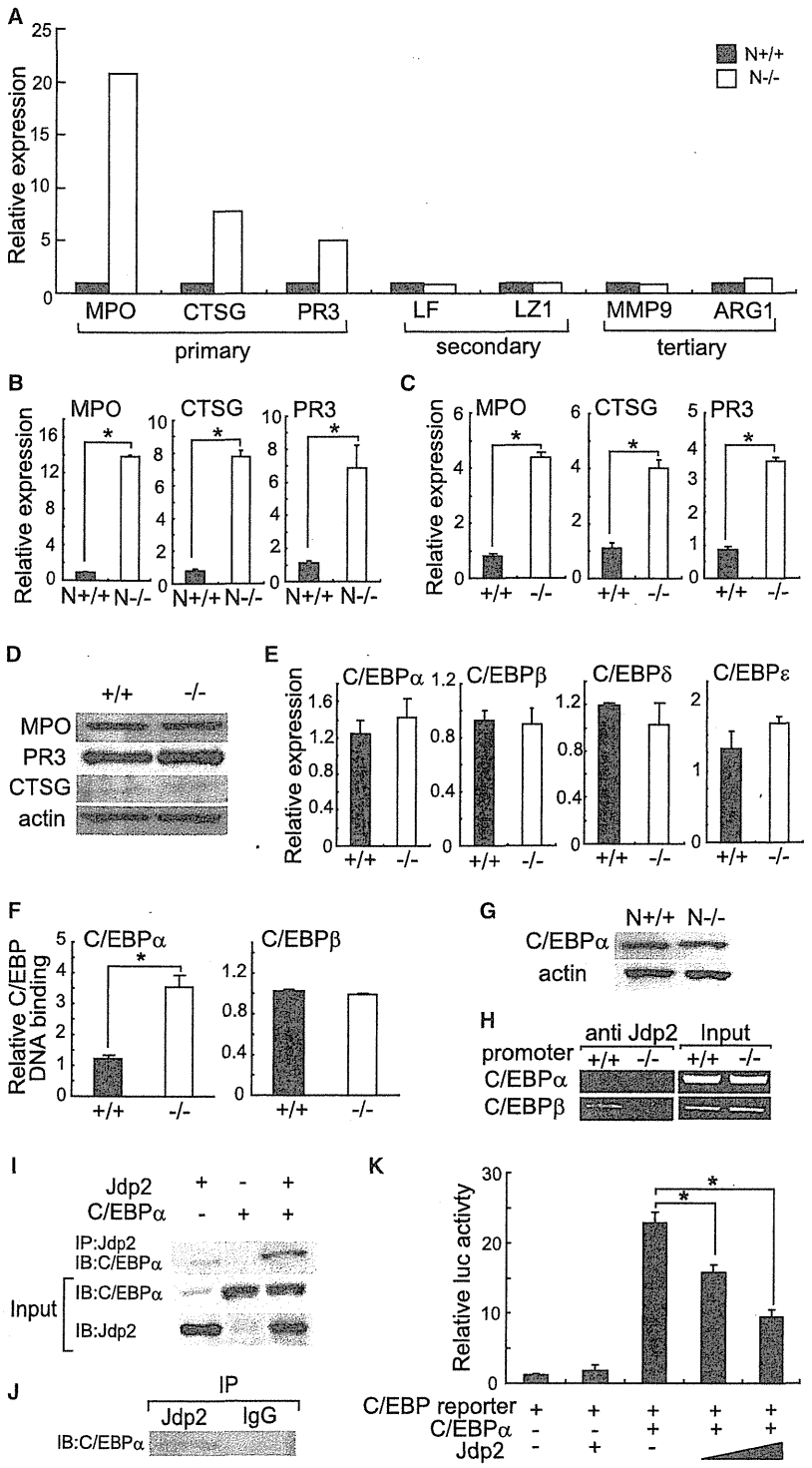

Figure 5. Aberrant mRNA Levels of Primary Granule Genes in *Jdp2*$^{-/-}$ Neutrophils

(A) Primary, secondary, and tertiary granule mRNA levels in bone marrow CD11b^{+}Ly6C^{lo}Ly6G^{+} neutrophils (N+/+ and N−/−) analyzed by a microarray.

(B and C) MPO, CTSG, and PR3 mRNA levels in CD11b^{+}Ly6C^{lo}Ly6G^{+} neutrophils (N+/+ and N−/−) (B) and peritoneal neutrophils (C) measured by qPCR.

(D) Primary granule protein levels in peritoneal neutrophils from wild-type and *Jdp2*$^{-/-}$ mice.

(E) C/EBP gene family mRNA levels in peritoneal neutrophils from wild-type and *Jdp2*$^{-/-}$ mice measured by qPCR.

(F) DNA-binding activities of C/EBPα and C/EBPβ in wild-type and *Jdp2*$^{-/-}$ peritoneal neutrophils measured with a TransAM Transcription Factor Assay Kit.

(G) C/EBPα protein levels in nuclear extracts from wild-type and *Jdp2*$^{-/-}$ peritoneal neutrophils analyzed by immunoblotting.

(H) ChIP analyses with a Jdp2 Ab of lysates from wild-type and *Jdp2*$^{-/-}$ peritoneal neutrophils. C/EBPα and C/EBPβ promoter regions were detected by PCR.

(I) 293T cells were transfected with the indicated pCMV expression vectors. After anti-Jdp2 immunoprecipitation (IP), input and immunoprecipitates were analyzed by immunoblotting with C/EBPα and Jdp2 Abs.

(J) Wild-type peritoneal neutrophils were lysed. After anti-Jdp2 and control IgG IP, immunoprecipitates were analyzed by immunoblotting with a C/EBPα Ab.

(K) Luciferase assays examining the effects of Jdp2 on the transcriptional activity of C/EBPα.

Error bars, SE (n = 3). *p < 0.05.

direct binding between Jdp2 and the ATF3 promoter (Figure 6F). Furthermore, we found that Jdp2 overexpression in wild-type neutrophils suppressed ATF3 promoter acetylation (Figure 6G).

Finally, to determine whether increased ATF3 expression affected neutrophil differentiation, we infected wild-type bone marrow cells with a retrovirus encoding ATF3 and GFP or GFP alone and analyzed the cells by FACS after 5 days as described earlier. Intriguingly, neutrophils infected with the ATF3-GFP retrovirus showed decreased Ly6G expression levels but unchanged cellular morphology, compared with GFP-alone control cells (Figure 6H). Thus, ATF3 is a negative regulator of neutrophil differentiation, and its expression is strictly regulated by Jdp2.

Jdp2$^{-/-}$ Mice Are Highly Susceptible to Bacterial and Fungal Infection

Because decreased neutrophil function is an important risk factor for *C. albicans* infection, we checked the susceptibility of *Jdp2*$^{-/-}$ mice to *C. albicans* challenge (Figures 7A–7C). We observed a slight but significant increase in *C. albicans* susceptibility in *Jdp2*$^{-/-}$

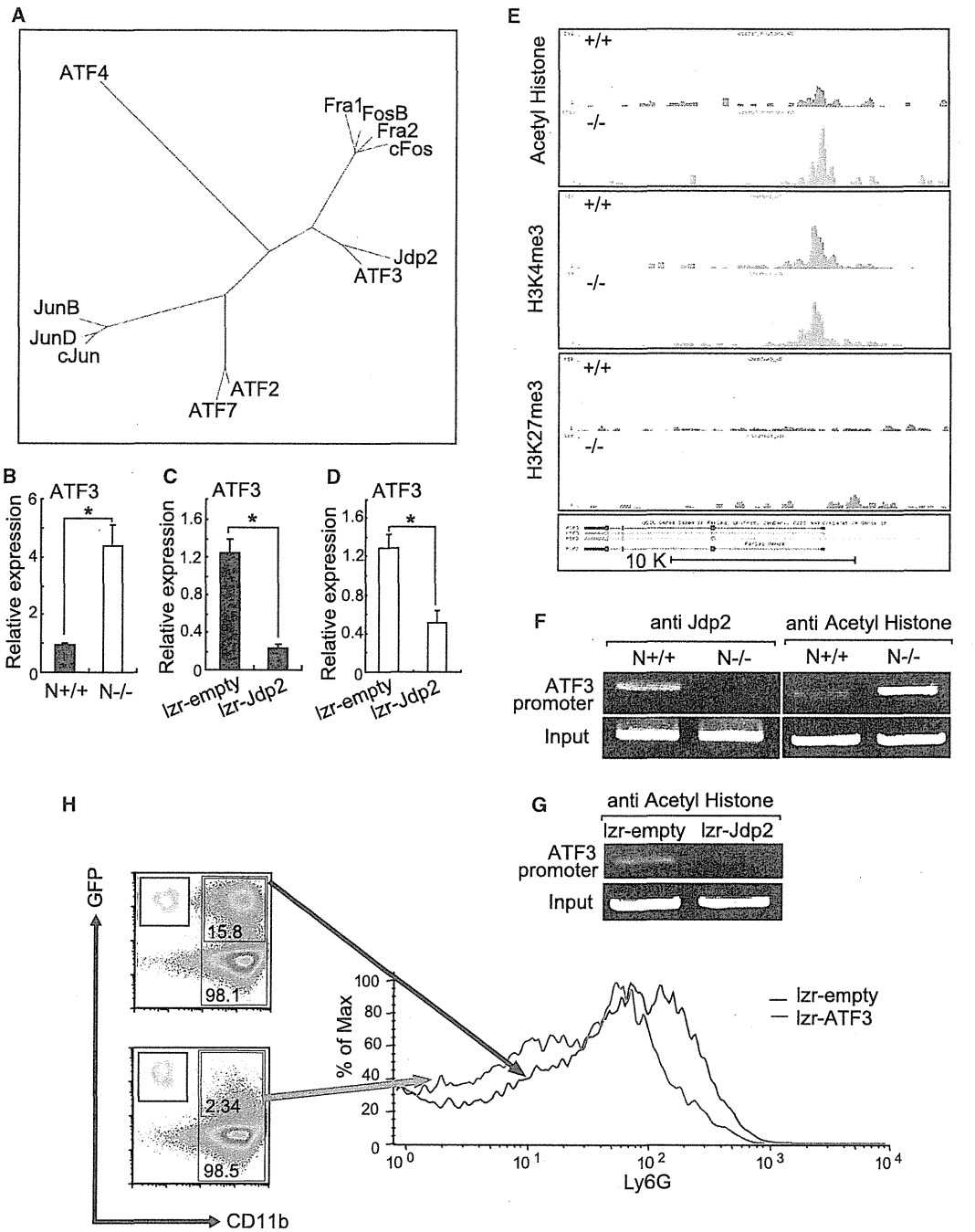

Figure 6. ATF3 Is a Target of Jdp2 and Modulates Ly6G Surface Expression

(A) Phylogenetic tree for AP-1 family proteins and Jdp2.

(B) ATF3 mRNA levels in bone marrow $CD11b^{+}Ly6C^{lo}Ly6G^{+}$ neutrophils (N+/+ and N−/−) analyzed by qPCR.

(C and D) Wild-type (C) and *Jdp2*$^{-/-}$ (D) bone marrow cells were infected with a retrovirus encoding Jdp2 and GFP (Izr-Jdp2) or GFP alone (Izr-empty) and cultured with G-CSF. After 5 days, the cells were harvested and $CD11b^{+}GFP^{+}$ cells were sorted. ATF3 mRNA levels were measured by qPCR.

(E) ChIP-seq enrichment profiles for acetyl-histone, H3K4me3, and H3K27me3 at the ATF3 locus in wild-type and *Jdp2*$^{-/-}$ peritoneal neutrophils.

(F) ChIP analyses with Jdp2 and acetyl-histone Abs of lysates from wild-type and *Jdp2*$^{-/-}$ bone marrow $CD11b^{+}Ly6C^{lo}Ly6G^{+}$ neutrophils (N+/+ and N−/−). DNA fragments of the ATF3 promoter region were detected by PCR.

(G) ChIP analyses with an acetyl-histone Ab of lysates in (C). DNA fragments of the ATF3 promoter region were detected by PCR.

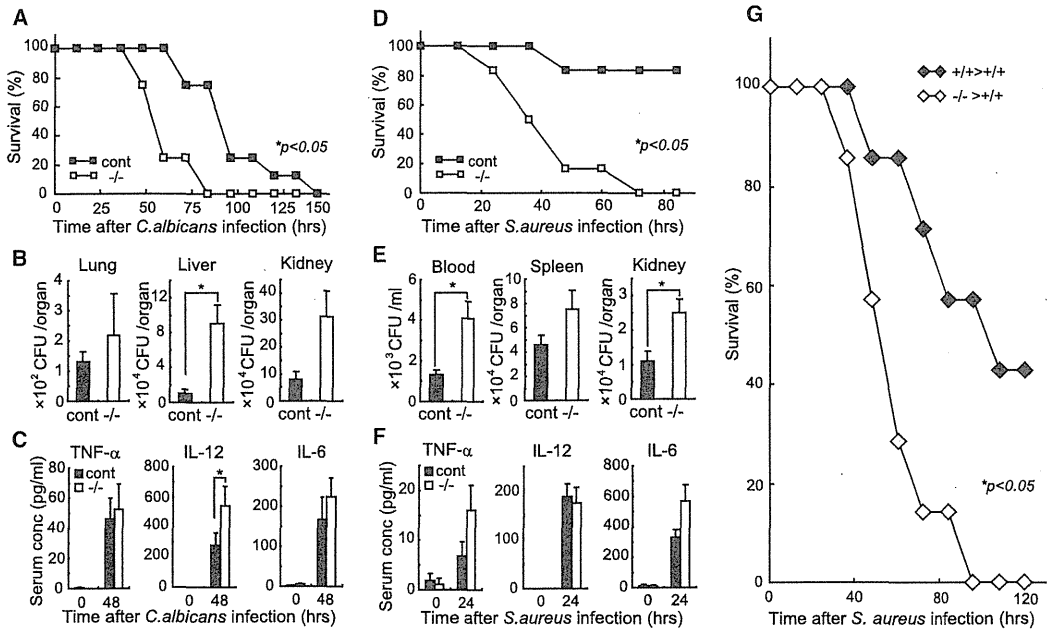

Figure 7. *Jdp2*$^{-/-}$ Mice Are Susceptible to Infection

(A–C) *C. albicans* was intravenously injected into *Jdp2*$^{+/+}$*Jdp2*$^{+/-}$ mice (control, n = 8) and *Jdp2*$^{-/-}$ mice (–/–, n = 8) and the mice were monitored (A). *Jdp2*$^{-/-}$ mice showed significantly worse survival than control mice ($p < 0.05$). CFU in the indicated organs (B) and serum cytokine levels (C) were determined at 36 hr after infection.

(D–F) *S. aureus* was intravenously injected into *Jdp2*$^{+/+}$*Jdp2*$^{+/-}$ mice (control, n = 6) and *Jdp2*$^{-/-}$ mice (–/–, n = 6) and the mice were monitored (D). *Jdp2*$^{-/-}$ mice showed significantly worse survival than control mice ($p < 0.05$). CFU in the indicated organs (E) and serum cytokine levels (F) were determined at 36 hr after infection.

(G) *S. aureus* was intravenously injected into wild-type mice reconstituted by transplantation of wild-type (+/+ > +/+, n = 7) or *Jdp2*$^{-/-}$ (–/– > +/+, n = 7) bone marrow and the mice were monitored. The survival was significantly worse in –/– > +/+ mice than in +/+ > +/+ mice ($p < 0.05$).

Error bars, SE (n = 4 unless indicated). *$p < 0.05$.

mice (Figure 7A), which showed elevated numbers of *C. albicans* CFU in their liver compared with wild-type mice (Figure 7B). The serum IL-12 levels were significantly elevated in *Jdp2*$^{-/-}$ mice, compared with wild-type mice, but the serum TNF-α and IL-6 levels were comparable (Figure 7C). We also infected *Jdp2*$^{-/-}$ and wild-type mice with *S. aureus* (Figures 7D–7F). Surprisingly, *Jdp2*$^{-/-}$ mice were highly susceptible to *S. aureus* infection, compared with wild-type mice (Figure 7D). *Jdp2*$^{-/-}$ mice showed significantly elevated numbers of *S. aureus* CFU in their blood and kidneys, compared with wild-type mice (Figure 7E). In contrast, the serum cytokine levels were not significantly altered (Figure 7F). To evaluate the relevance of hematopoietic Jdp2 deficiency to protective immunity against pathogens, we irradiated wild-type mice and reconstituted them with bone marrow from wild-type or *Jdp2*$^{-/-}$ mice (Figure 7G). Chimeric mice lacking Jdp2 in their hematopoietic system showed significantly increased susceptibility to *S. aureus* (Figure 7G). To evaluate the importance of lymphocytes in protective immunity against *S. aureus* infection in our experimental model, we depleted T and B cells in wild-type mice reconstituted with bone marrow from wild-type mice by using CD3 and CD20 Abs (Figure S6A). However, this depletion had no effect on survival in response to *S. aureus* (Figure S6B). Thus, we think our infection model reflects the function of cells other than T and B cells. Next, we depleted neutrophils in bone marrow chimeric mice by using a Ly6G Ab (Figure S6C). We infected the neutrophil-depleted chimeric mice with *S. aureus* and observed no significant difference in *S. aureus*-induced lethality between wild-type and *Jdp2*$^{-/-}$ chimeric mice (Figure S6D). Thus, these findings suggest that the increased susceptibility to *S. aureus* in *Jdp2*$^{-/-}$ mice is due to an abnormal neutrophil phenotype.

DISCUSSION

We have demonstrated that Jdp2 plays a critical role in osteoclastogenesis in vivo. We also discovered that in vitro osteoclastogenesis was completely abolished in *Jdp2*$^{-/-}$ cells. Furthermore, RANKL-mediated Jdp2 induction appeared to be

(H) Wild-type bone marrow cells were infected with a retrovirus encoding ATF3 and GFP (lzr-ATF3) or GFP alone (lzr-empty) and cultured with G-CSF. After 5 days, CD11b^{+}GFP^{+} cells were gated and Ly6G expression levels were quantified by FACS. Gated cells were also sorted and stained by May-Grunwald-Giemsa (upper left insets in the scatter plots).

Error bars, SE (n = 3). *$p < 0.05$.